Cell Reports

Article

De novo steroidogenesis in tumor cells drives bone metastasis and osteoclastogenesis

Graphical abstract

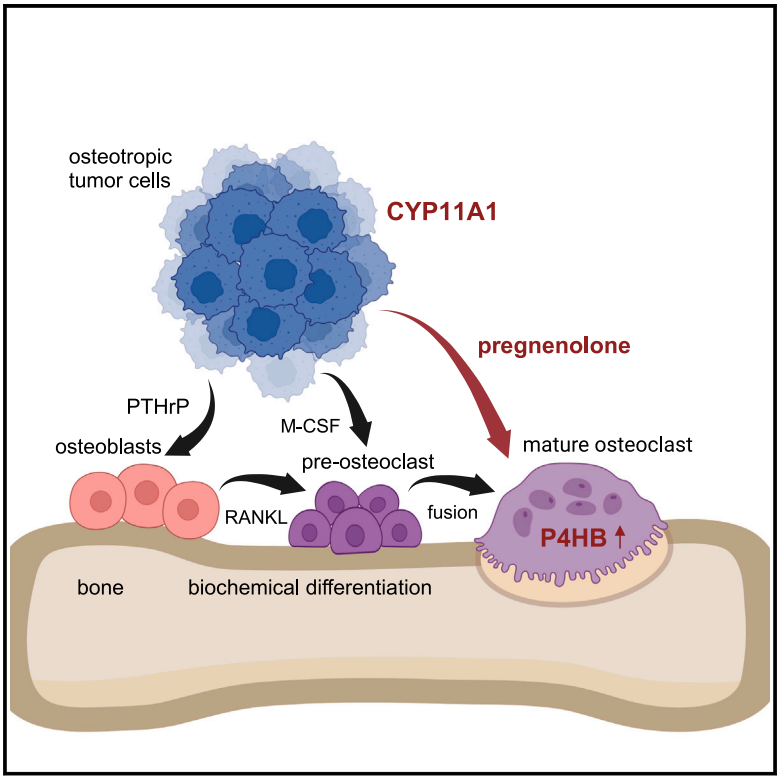

Authors

Luca F. Sandor, Joon B. Huh, Peter Benko, ..., Natalie Z.M. Homer, Bidesh Mahata, David S. Gyori

Correspondence

gyori.david@semmelweis.hu

In brief

Sandor et al. show that CYP11A1-mediated *de novo* steroidogenesis in osteotropic tumor cells drives bone metastasis and osteoclastogenesis in both humans and mice. They identify pregnenolone, product of CYP11A1 activity, as a potential cancer-cell-derived regulator of osteoclastogenesis, able to stimulate the fusion of osteoclasts via interaction with the P4HB molecule.

Highlights

- Osteotropic tumors express CYP11A1 and *de novo* synthetize the steroid pregnenolone
- Intratumoral CYP11A1 promotes bone metastasis formation and tumor-induced osteolysis
- Pregnenolone drives osteoclastogenesis and fusion of osteoclasts via P4HB molecule
- Osteotropic human cancer cells produce pregnenolone and enhance osteoclastogenesis

Sandor et al., 2024, Cell Reports *43*, 113936
March 26, 2024
https://doi.org/10.1016/j.celrep.2024.113936

CellPress

Cell Reports

CellPress
OPEN ACCESS

Article

De novo steroidogenesis in tumor cells drives bone metastasis and osteoclastogenesis

Luca F. Sandor,[1] Joon B. Huh,[1] Peter Benko,[1] Toru Hiraga,[2] Szilard Poliska,[3] Csaba Dobo-Nagy,[4] Joanna P. Simpson,[5] Natalie Z.M. Homer,[5,6] Bidesh Mahata,[7] and David S. Gyori[1,8,*]

[1]Department of Physiology, Semmelweis University School of Medicine, 1094 Budapest, Hungary
[2]Department of Histology and Cell Biology, Matsumoto Dental University, Shiojiri, Nagano 399-0781, Japan
[3]Department of Biochemistry and Molecular Biology, Faculty of Medicine, University of Debrecen, 4032 Debrecen, Hungary
[4]Department of Oral Diagnostics, Semmelweis University School of Dentistry, 1088 Budapest, Hungary
[5]Mass Spectrometry Core, Edinburgh Clinical Research Facility, Queen's Medical Research Institute, University of Edinburgh, EH16 4TJ Edinburgh, UK
[6]University of Edinburgh/BHF Centre for Cardiovascular Sciences, Queen's Medical Research Institute, University of Edinburgh, EH16 4TJ Edinburgh, UK
[7]Department of Pathology, University of Cambridge, Cambridge CB21QP Cambridgeshire, UK
[8]Lead contact
*Correspondence: gyori.david@semmelweis.hu
https://doi.org/10.1016/j.celrep.2024.113936

SUMMARY

Osteoclasts play a central role in cancer-cell-induced osteolysis, but the molecular mechanisms of osteoclast activation during bone metastasis formation are incompletely understood. By performing RNA sequencing on a mouse breast carcinoma cell line with higher bone-metastatic potential, here we identify the enzyme CYP11A1 strongly upregulated in osteotropic tumor cells. Genetic deletion of *Cyp11a1* in tumor cells leads to a decreased number of bone metastases but does not alter primary tumor growth and lung metastasis formation in mice. The product of CYP11A1 activity, pregnenolone, increases the number and function of mouse and human osteoclasts *in vitro* but does not alter osteoclast-specific gene expression. Instead, tumor-derived pregnenolone strongly enhances the fusion of pre-osteoclasts via prolyl 4-hydroxylase subunit beta (P4HB), identified as a potential interaction partner of pregnenolone. Taken together, our results demonstrate that *Cyp11a1*-expressing tumor cells produce pregnenolone, which is capable of promoting bone metastasis formation and osteoclast development via P4HB.

INTRODUCTION

Osteolytic bone metastases, where bone tissue is destroyed, lead to pathological fractures and increased patient mortality.[1–3] Although osteoclasts, the unique bone-resorbing cells of hematopoietic origin, are essential for pathological bone loss, the molecular mechanisms directing osteoclast differentiation during skeletal lesion formation are largely unknown. The aim of our experiments was to identify tumor-cell-derived factors, which are capable of promoting the development and function of osteoclasts during bone metastasis.

Although cancer cells forming skeletal lesions are able to exert proteolytic activity to some level, they cannot break down the bone matrix.[4] The digestion of both the organic and inorganic components of the bone is then carried out by osteoclasts, the sole bone-resorbing cells of the human body, accumulating in close proximity to the osteotropic tumor cells.[5] Osteoclast development is directed by two main growth factors, namely receptor activator of nuclear factor κB ligand (RANKL) and macrophage colony-stimulating factor (M-CSF), which are provided by stromal cells, such as osteoblasts and osteocytes under non-pathological conditions.[6] The first phase of osteoclast development is then determined by the expression of various osteoclast-specific genes, such as tartrate-resistant acidic phosphatase (TRAP), in pre-osteoclasts.[7] During the second phase of osteoclast differentiation, fusion of these pre-osteoclasts occurs and leads to the development of large, multinucleated, mature osteoclasts.[8] Finally, those mature polykarions spread over the bone surface by forming actin rings and sealing zones in order to degrade the bone matrix via the parallel release of digestive enzymes and hydrochloric acid.[9]

Solid tumors capable of forming osteolytic bone metastases were previously considered to induce osteoclast differentiation indirectly via the activation of osteoblasts.[10] During this process, cancer-cell-derived parathyroid hormone-related peptide (PTHrP) induces the expression of RANKL on osteoblasts, which in turn drives the differentiation of multinucleated osteoclast from myeloid precursors.[11] Mature osteoclasts then resorb the bone matrix and allow tumor cells to grow and spread within the tissue. In this study, our results suggest that osteoclast differentiation can also be directly initiated by the cancer cells themselves. Here, we demonstrate that steroids *de novo* produced by *Cyp11a1*-expressing tumor cells are able to support bone metastasis formation and the development and resorptive

function of osteoclasts in both humans and mice. We identify pregnenolone, a potential tumor-cell-derived regulator of osteoclastogenesis, which is capable of promoting the fusion of osteoclasts via the prolyl 4-hydroxylase subunit beta (P4HB) molecule.

RESULTS

Tumor-cell-derived soluble factors are capable of promoting osteoclast development *in vitro*

The E0771/bone breast carcinoma cell line with higher bone-metastatic potential compared to the parental cell line (E0771/Pa) was established by sequential *in vivo* selection in mice.[12] After culturing the cells in the presence of serum-free medium for 24 h, supernatants of E0771/bone and E0771/Pa cells were centrifuged, filtered, and incubated with mouse bone-marrow-derived osteoclast precursors. To our surprise, supernatants from E0771/bone cells were able to strongly promote the development of multinucleated, TRAP-positive giant cells (Figures 1A and 1B) comparable to those from recombinant M-CSF- and soluble RANKL-treated cultures. Those osteoclast-like cells induced by E0771/bone (but not by E0771/Pa) supernatants were able to resorb hydroxyapatite surfaces (Figures 1A and 1B). Further, the effect of tumor cell supernatants on osteoclasts was likely independent of soluble RANKL, as we could not detect any RANKL secreted by the E0771/bone cancer cells *in vitro* by ELISA (Figure S1A). Taken together, by using a bone-metastatic clone of E0771 breast carcinoma cells (E0771/bone), we were able to demonstrate the presence of tumor-cell-derived soluble factors capable of inducing *in vitro* development and function of bone-marrow-derived osteoclasts.

The steroidogenic enzyme CYP11A1 is strongly upregulated in the osteotropic tumor cells

Next, we compared the global gene expression profiles of E0771/bone and E0771/Pa cells by RNA sequencing. Using next-generation sequencing performed on an Illumina platform, we were able to identify approximately 200 differently regulated genes, about 150 of which were upregulated and almost 50 of which were downregulated in the E0771/bone cells compared to E0771/Pa cells (Figure 1C). Gene Ontology and pathway enrichment analysis showed that genes involved in the regulation of bone homeostasis (e.g., bone morphogenetic proteins, Wnt and Notch signaling pathways) were upregulated in E0771/bone cells (Figure 1D). However, one of the genes strongly upregulated in the E0771/bone cells was *Cyp11a1*, encoding the steroidogenic enzyme CYP11A1 (Figures 1E and S1B). This enzyme, a member of the cytochrome P450 family, is situated in the mitochondrial inner membrane and catalyzes the first and enzymatically rate-limiting step in the synthesis of steroid hormones by converting cholesterol to pregnenolone (Figure 1F). This so-called *de novo* steroidogenesis classically takes places in the adrenal gland, gonads, and placenta; however, more recent data suggest that extraglandular steroidogenesis can also occur in several other tissues under physiological and pathological conditions.[13–21] We were therefore interested to see whether this enzyme is functional in the osteotropic tumor cells and whether its presence could lead to the generation of its product pregnenolone. To this end, we measured the concentration of pregnenolone in the supernatants of different mouse cancer cell lines capable of forming osteolytic bone metastases by two techniques, ELISA and liquid chromatography-tandem mass spectrometry (LC-MS/MS). We also profiled steroids using LC-MS/MS. As shown in Figure 1G, E0771/bone breast carcinoma cells secreted more pregnenolone than E0771/Pa cells, and B16F10 malignant melanoma cells secreted the highest levels of pregnenolone into their supernatants. However, tumor cell lines, which form very few or no bone metastases, such as MC38 colorectal carcinoma and LLC (Lewis lung carcinoma) cells, secreted low levels or no pregnenolone into their supernatants. Further, we could not detect the expression of the enzymes *Cyp17a1* (encoding 17-hydroxylase) and *Hsd3b* (encoding 3β-hydroxysteroid dehydrogenase) (Figure S1C) or the presence of any other steroids, including aldosterone, corticosterone, 17β-estradiol, progesterone, 17-OH pregnenolone, DHEA, androstenedione, 5α-dihydrotestosterone, and testosterone, secreted by the osteotropic tumor cells measured by ELISA or targeted steroid profiling LC-MS/MS method (Figures S1D–S1F). Finally, we also detected high levels of pregnenolone (but not androstenedione, cortisol, DHEA, 17β-estradiol, estrone, estriol, progesterone, 5α-dihydrotestosterone, or testosterone) in the extracellular fluid (ECF) of E0771/bone and B16F10 (but not E0771/Pa) primary tumors by ELISA and targeted LC-MS/MS (Figures S1G–S1I). Taken together, our results indicate that different osteotropic tumor cells express the steroidogenic enzyme CYP11A1 and that its product, pregnenolone, is present in high concentrations in their environment.

Genetic deficiency of CYP11A1 in tumor cells leads to decreased bone metastasis formation

Having found that high levels of pregnenolone are secreted into the culture supernatant and ECF by different mouse solid tumor cell lines, we next asked whether *Cyp11a1*-expressing cancer-cell-derived pregnenolone can support bone metastasis formation *in vivo*. To this end, we disrupted the gene encoding CYP11A1 using CRISPR-Cas9 mutagenesis in B16F10 cells. We confirmed that *Cyp11a1*$^{-/-}$ B16F10 cells are not expressing CYP11A1 at the protein level (Figure S2A) and are not able to secrete pregnenolone into the culture supernatant (Figure S2B). However, we detected no significant difference between the growth rates of parental (wild-type [WT]) and *Cyp11a1*$^{-/-}$ B16F10 cells *in vitro* (Figure S2C).

Further, when implanting WT and *Cyp11a1*$^{-/-}$ B16F10 cells intradermally into C57BL/6 mice, we could not detect any significant difference between the *in vivo* growth rates of the two genotypes (Figures 2A and 2B). Moreover, intravenous injection of WT and *Cyp11a1*$^{-/-}$ B16F10 cells resulted in no difference in the level of lung metastasis formation as well (Figures 2C and 2D). However, to our surprise, when injecting WT and *Cyp11a1*$^{-/-}$ tumor cells into the caudal artery of C57BL/6 mice to induce bone metastasis formation in the long bones (femurs and tibias) of the hind limbs, almost no tumor deposits were macroscopically visible in mice injected with *Cyp11a1*$^{-/-}$ B16F10 cells, while melanin-rich tumor deposits were clearly seen in mouse long bones injected with *Cyp11a1*$^{+/+}$ B16F10

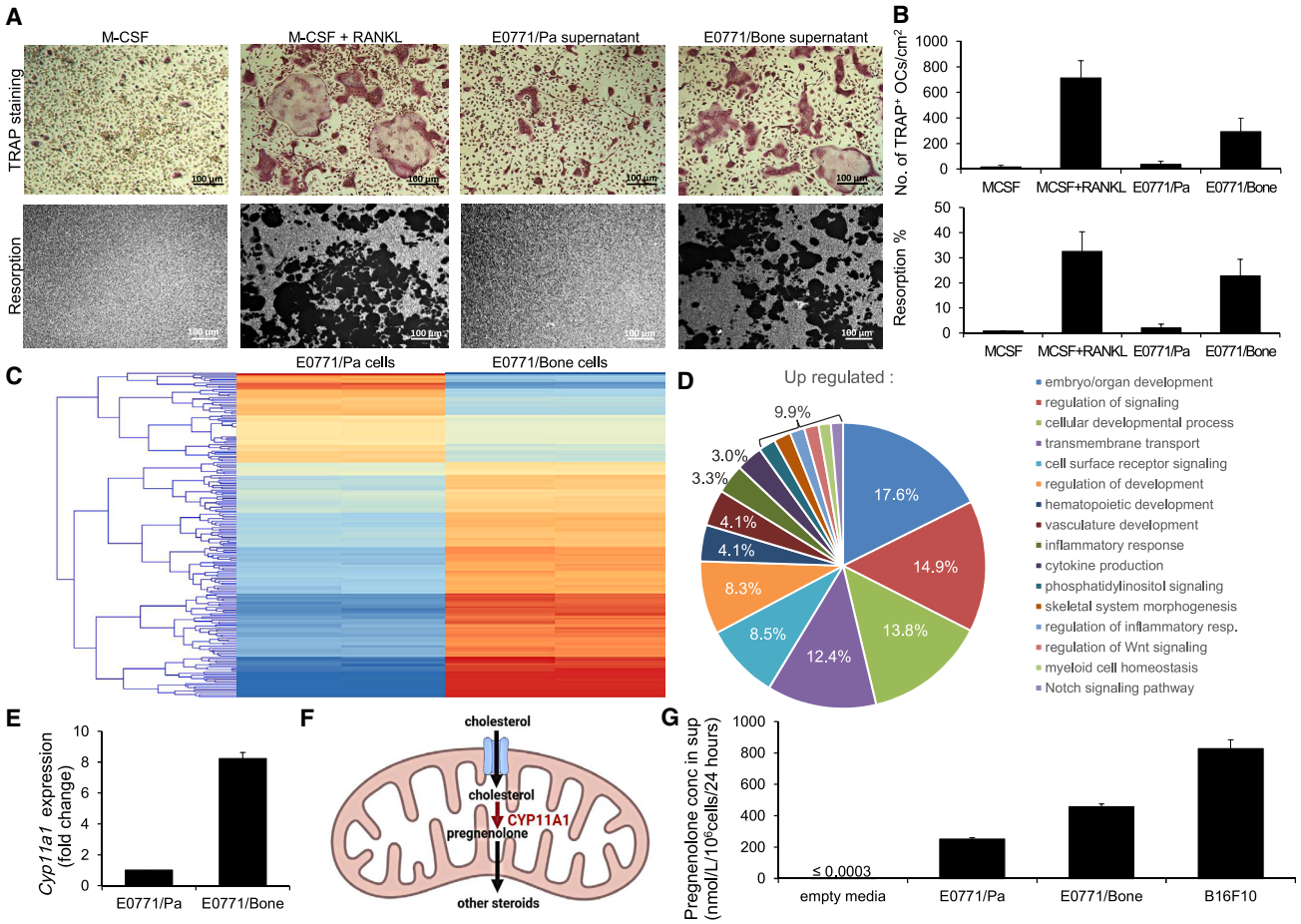

Figure 1. CYP11A1 catalyzes *de novo* steroidogenesis in osteotropic tumor cells

(A and B) Representative images (A) and quantification (B) of TRAP-stained cell cultures (top) and resorption on artificial hydroxyapatite surface (bottom) by wild-type (WT) mouse bone-marrow-derived macrophages cultured for 3 days in the presence of 20 ng/mL M-CSF with or without 20 ng/mL RANKL or in the supernatants of E0771/Pa or E0771/bone cells. Scale bars represent 100 μm.

(C) Heatmaps of significantly up- (red) and downregulated (blue) genes in E0771/bone cells compared to E0771/Pa cells identified by RNA sequencing, followed by moderated t test and Benjamini-Hochberg false discovery rate.

(D) List of group of genes upregulated in E0771/bone cells compared to E0771/Pa cells identified by Gene Ontology and pathway enrichment analysis.

(E) Analysis of gene expression of *Cyp11a1* in E0771/Pa vs. E0771/bone cells.

(F) Schematic representation of the role of CYP11A1 within the mitochondria of the cells. Image was created in BioRender (www.biorender.com).

(G) Levels of pregnenolone in the supernatants of E0771/Pa, E0771/bone, and B16F10 cells measured by liquid chromatography-tandem mass spectrometry (LC-MS/MS).

Bar graphs show mean and SD of data from 3 independent experiments.

cancer cells (Figures 2E and 2F). Importantly, administration of exogenous pregnenolone restored bone tumor growth of *Cyp11a1*$^{-/-}$ B16F10 cells (Figure S2D). Further, aminoglutethimide, a pharmacological inhibitor of CYP11A1, significantly decreased bone metastasis formation in mice injected with E0771/bone tumor cells (Figures S2E and S2F). Moreover, when E0771/Pa cells—which spontaneously develop very few or no bone metastasis—were injected into the caudal artery of the mice, pregnenolone treatment alone could lead to the formation of osteolytic skeletal lesions (Figures S2G and S2H). Similarly, when injecting *Cyp11a1*-overexpressing TRAMP-C1 prostate cancer cells into the experimental animals, significantly more bone metastases were detected (Figures S2I–S2K). These results indicate that *Cyp11a1* expressed in the solid tumor cells plays an important role in promoting bone metastasis *in vivo*.

Genetic deficiency of CYP11A1 in tumors protects mice from osteoclast-mediated osteolysis

To test the role of CYP11A1 in the process of bone metastasis formation, we analyzed trabecular bone structure of the distal metaphysis of the femurs of mice injected with WT and *Cyp11a1*$^{-/-}$ B16F10 cells using micro-computed tomography (micro-CT) and histomorphometric analyses. As shown in Figure 3A, more trabeculae were seen in a three-dimensional

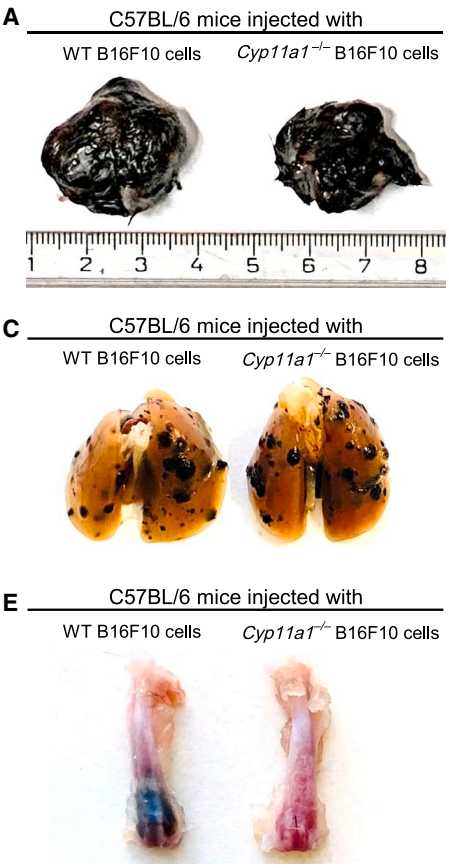

Figure 2. CYP11A1 in osteotropic tumor cells drives bone metastasis formation

Representative images (A, C, and E) and quantification (B, D, and F) of primary tumor growth and lung metastasis and bone metastasis formation by WT and CRISPR-Cas9-engineered *Cyp11a1*$^{-/-}$ B16F10 cells injected intradermally (A and B), into the tail vein (C and D), or into the caudal artery (E and F) of C57BL/6 mice.

Data were obtained from 6 mice per group. Error bars represent SEM. *p < 0.05; n.s., not significant.

reconstitution of an axial cylinder of the femurs of *Cyp11a1*$^{-/-}$-tumor-injected animals compared to the ones injected with *Cyp11a1*$^{+/+}$ B16F10 cells. Quantification of the entire trabecular area (Figure 3B) revealed a significantly increased bone volume/total volume (BV/TV) in the femurs of animals injected with *Cyp11a1*$^{-/-}$ B16F10 cells compared to the WT-tumor-injected ones, which was primarily due to increased trabecular number rather than increased thickness of the individual trabeculae (Figure 3B).

We also performed histological and histomorphometric analyses on the trabecular bone of the distal femurs of mice injected with WT and *Cyp11a1*$^{-/-}$ B16F10 cells. As shown in Figure 3C, less tumor mass and more trabeculae were seen in the histological sections of the femurs of animals injected with *Cyp11a1*$^{-/-}$ cancer cells compared to the ones injected with *Cyp11a1*$^{+/+}$ B16F10 cells. We next analyzed osteoclasts visible in the TRAP-stained sections (Figure 3D). There was a statistically significant reduction in the average number of osteoclasts per bone perimeter in mice injected with *Cyp11a1*$^{-/-}$ B16F10 cells (Figure 3E). In addition, we could detect a significant decrease in the level of C-terminal telopeptide, a marker of bone resorption in mice injected with *Cyp11a1*$^{-/-}$ B16F10 cell compared to the WT-tumor-injected ones (Figure 3F), but there was no difference in the level of bone formation marker osteocalcin (Figure 3G). Taken together, our data indicate that genetic deficiency of CYP11A1 in the osteotropic tumor cells protects mice from cancer-cell-induced, osteoclast-mediated osteolysis *in vivo*.

Pregnenolone promotes osteoclast development and function *in vitro*

As shown in Figures 4A and 4B, similar to E0771/bone, B16F10 WT tumor cell supernatants (but not B16F10 *Cyp11a1*$^{-/-}$ tumor cell supernatants) were also able to promote *in vitro* osteoclastogenesis to a level comparable with the effect of 20 ng/mL recombinant M-CSF and 20 ng/mL soluble RANKL. This effect of WT tumor cell supernatants was dose dependent (Figures S3A and S3B). Moreover, when co-culturing B16F10 cells with bone-marrow-derived macrophages, the osteotropic cancer cells were capable of inducing the development of large, multinucleated, TRAP-positive giant cells, which could also resorb the bone (Figures S3C–S3F). We were next interested in whether pregnenolone could be the soluble factor produced by the tumor cells responsible for this effect. Accordingly, bone-marrow-derived osteoclast precursor cultures were treated with different concentrations of pregnenolone following the induction of an osteoclast-specific gene expression program in the bone marrow cells by pre-treatment with 20 ng/mL M-CSF and RANKL. As shown in Figures 4C and 4D, pregnenolone in the nanomolar concentration range dose-dependently increased the number and size of TRAP-positive, multinucleated osteoclasts compared to the control cultures treated with 20 ng/mL recombinant M-CSF and RANKL. Interestingly, corticosterone (but not 17-OH pregnenolone, progesterone, DHEA, or androstenedione) had a similar effect on *in vitro* osteoclastogenesis (Figures S3G and S3H), but we could not detect it in the tumor cell supernatants (Figure S1D). On the other hand, higher pregnenolone concentrations within the micromolar range had an opposite effect and rather decreased the number of osteoclasts in the cultures (Figures 4C and 4D). Similar results were obtained when we tested the resorptive capacity of *in vitro* osteoclast cultures in the presence of pregnenolone on bovine bone slices. As shown in Figures 4C and 4E, pregnenolone dose-dependently increased the function of osteoclast in the nanomolar

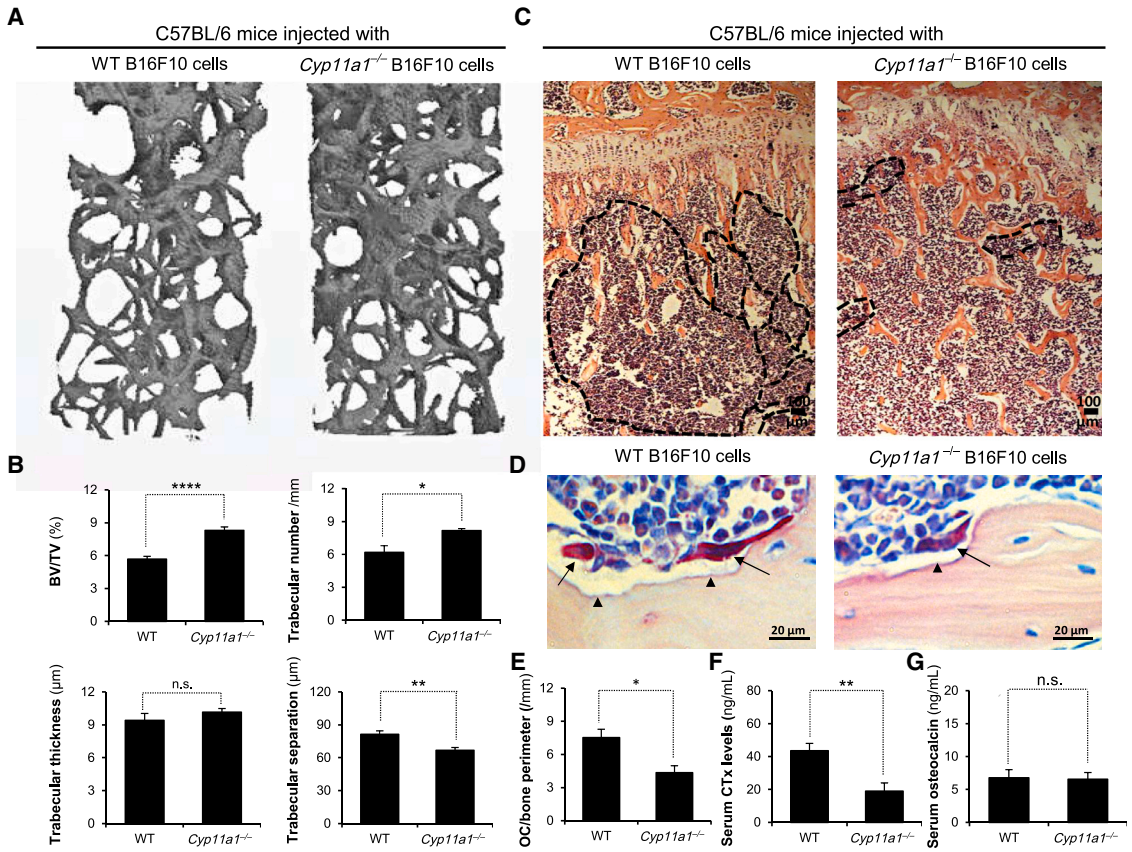

Figure 3. Genetic deficiency of CYP11A1 in tumors protects mice from osteoclast (OC)-mediated osteolysis

(A) Representative three-dimensional (3D) reconstitution of an axial cylinder of the trabecular area of the distal femoral metaphysis of 8- to 10-week-old C57BL/6 mice injected into the caudal artery with WT and *Cyp11a1*$^{-/-}$ B16F10 cells.

(B) Quantitative micro-CT analysis of the trabecular bone architecture of mice injected with WT and *Cyp11a1*$^{-/-}$ B16F10 cells. BV/TV, percentage of bone volume (bone volume/total volume).

(C and D) Representative images (C) of the trabecular area of mice injected with WT and *Cyp11a1*$^{-/-}$ B16F10 tumor cells. Insets (D) show enlarged views of TRAP-stained sections with OCs (arrows) and resorption pits (arrowheads). Scale bars represent 100 (C) and 20 μm (D).

(E) Histomorphometric analysis of the trabecular bone architecture and the number of OCs per bone perimeter.

(F and G) Levels of C-terminal telopeptide (CTx) (F) and osteocalcin (G) in the sera of mice injected with WT and *Cyp11a1*$^{-/-}$ B16F10 tumor cells.

Data were obtained from 6 mice per group. Error bars represent SEM. *p < 0.05, **p < 0.01, and ****p < 0.0004; n.s., not significant.

concentration range. To ensure their function, mature osteoclasts form actin rings to seal the resorption pits. In line with this important function, significantly more continuous F-actin rings were observed in osteoclast cultures treated with 50–500 nM pregnenolone compared to the control-treated cultures (Figures 4C and 4F). In contrast, significantly less resorption pits and slightly lower numbers of actin rings were seen in the osteoclast cultures treated with ≥1 μM pregnenolone (Figures 4C, 4E, and 4F). The most likely explanation for this is that higher concentrations of pregnenolone decrease the survival of osteoclast-lineage cells. As shown in Figure 4G, approximately 90% of pre-osteoclasts were negative for the apoptosis marker Annexin V and the necrosis marker 7-AAD under lower pregnenolone concentrations within the nanomolar range, whereas 1 μM pregnenolone triggered apoptosis and necrosis of the cells.

In summary, pregnenolone in the concentration range secreted by osteotropic tumor cells strongly promotes the *in vitro* development, resorptive function, and actin ring formation of osteoclasts but does not affect the survival, apoptosis, or necrosis of osteoclast-lineage cells.

Pregnenolone is not sufficient for osteoclast-specific gene expression

To understand the mechanism of how tumor-cell-derived pregnenolone drives the development of osteoclasts, we next tested the expression of osteoclast-specific genes. This process takes place during the biochemical maturation of osteoclast precursors, which is the early phase of osteoclastogenesis. To induce an osteoclast-specific gene expression program, mouse bone marrow progenitors were cultured in the presence of 20-20 ng/mL recombinant M-CSF and RANKL for 2 days and then in the presence of the indicated concentration of pregnenolone or vehicle for 3 more days. We used bone-marrow-derived macrophages cultured in the presence of M-CSF or pregnenolone alone as negative controls. As shown in Figure 5A, the

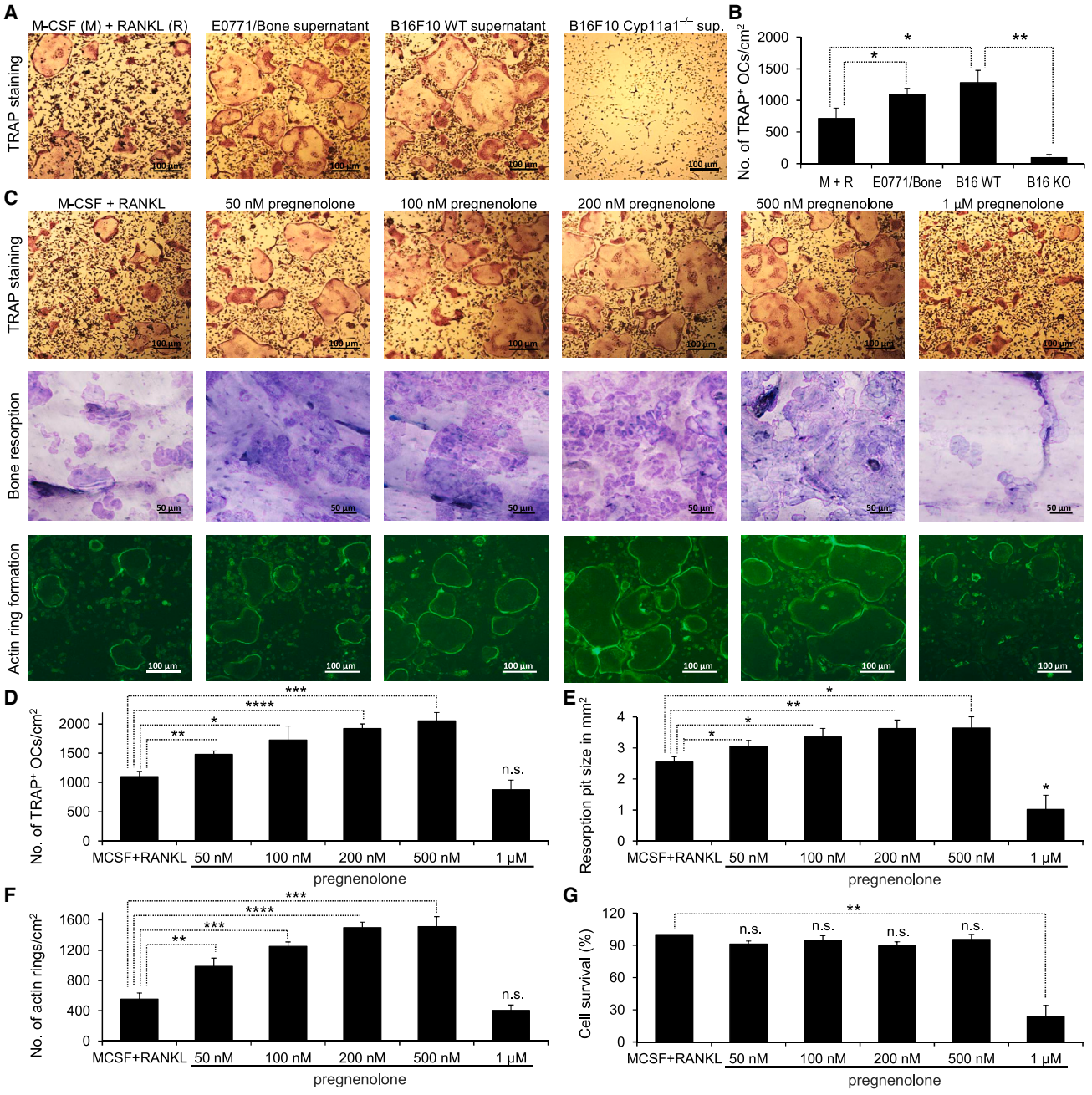

Figure 4. Pregnenolone promotes OC development and function *in vitro*

(A and B) Representative images (A) and quantification (B) of TRAP-stained cell cultures of WT mouse bone-marrow-derived macrophages cultured in the presence of 20 ng/mL M-CSF and 20 ng/mL RANKL or in the supernatants of E0771/bone, B16F10 WT, or *Cyp11a1*$^{-/-}$ cells. Scale bars represent 100 μm.

(C–F) Representative images (C) and quantification (D–F) of TRAP-stained cell cultures (C and D), *in vitro* resorption on bovine bone slices (C and E), and actin ring formation (C and F) by WT mouse bone-marrow-derived macrophages cultured for 2 days in the presence of 20 ng/mL M-CSF and 20 ng/mL RANKL and then for 3 (C, D, and F) or 11 (C and E) days in the presence of vehicle or the indicated concentration of pregnenolone. OCs are defined as TRAP-positive cells with 3 or more nuclei. Scale bars represent 100 (TRAP staining and actin ring formation) and 50 μm (bone resorption).

(G) Quantification of the percentage of surviving cells detected after the binding of Annexin-V-PE (apoptosis) and 7-AAD (necrosis) markers to WT bone-marrow-derived macrophages cultured for 2 days in the presence of 20 ng/mL M-CSF and 20 ng/mL RANKL and then for another 3 days with vehicle or the indicated concentration of pregnenolone. Surviving cells are defined as negative for both Annexin-V-PE and 7-AAD staining.

Bar graphs represent mean and SD of data from 3–6 independent experiments. *$p < 0.05$, **$p < 0.01$, ***$p < 0.002$, and ****$p < 0.0004$; n.s., not significant.

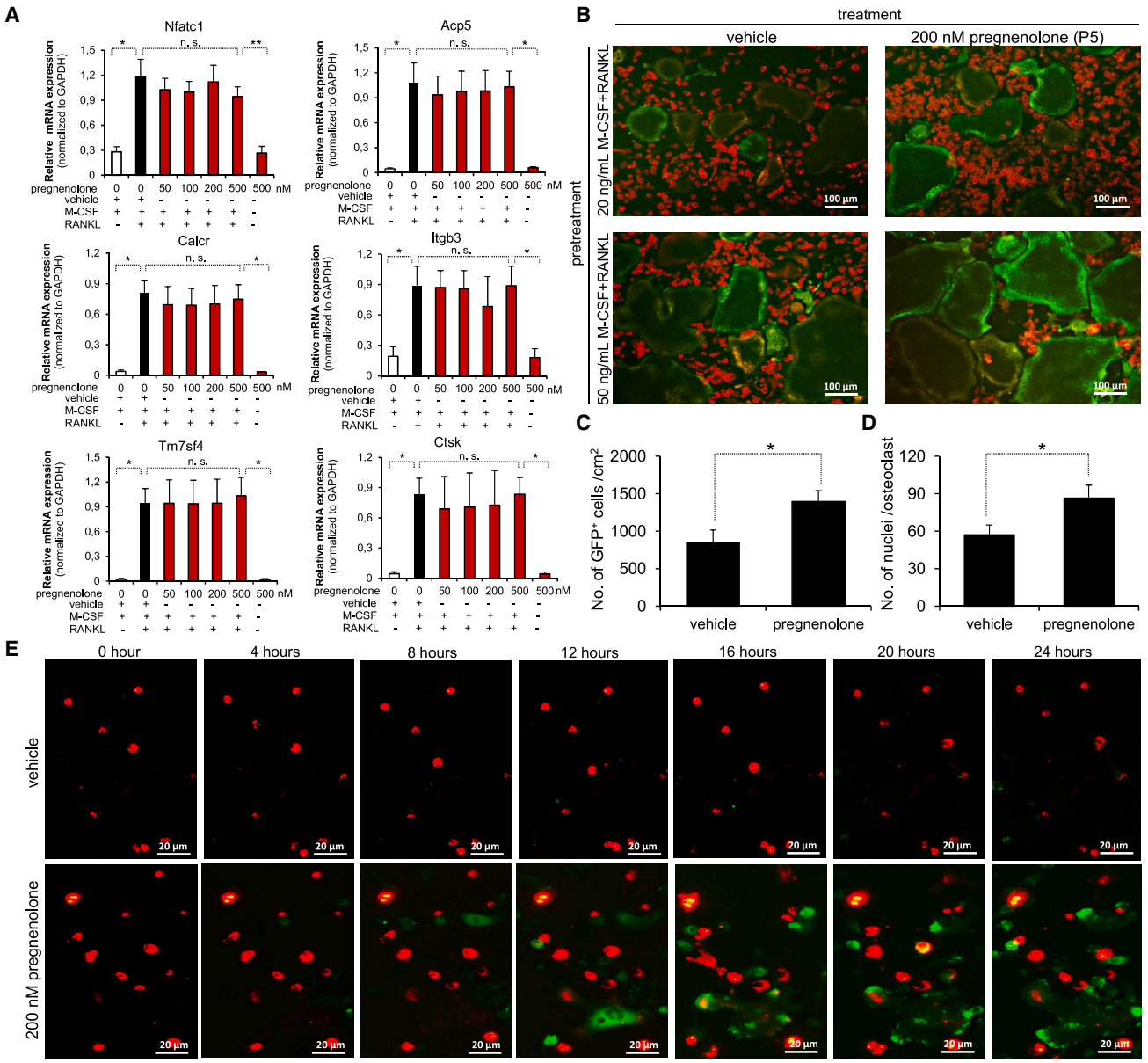

Figure 5. Pregnenolone drives the fusion of OCs, but it is dispensable for OC-specific gene expression

(A) Gene expression in WT mouse bone-marrow-derived progenitors cultured for 2 days in the presence of 20 and 20 ng/mL M-CSF and RANKL (OCs) or M-CSF (macrophages) or pregnenolone alone and then in the indicated concentrations of pregnenolone or vehicle for 3 days. The expressions of the *Nfatc1*, *Acp5*, *Calcr*, *Itgb3*, *Tm7sf4*, and *Ctsk* genes (encoding for NFATc1, TRAP, calcitonin receptor, integrin β_3, DC-STAMP, and cathepsin K, respectively) were determined by RT-qPCR.

(B and C) Representative images (B) and quantification of the number of GFP^+ cells (C) generated by co-culturing bone marrow cells from Ctsk-Cre and mTmG transgenic mice in the presence of 20 or 50 ng/mL M-CSF and 20 or 50 ng/mL RANKL for 2 days and then in the presence of vehicle or 200 nM pregnenolone for another 3 days. Scale bars represent 100 µm.

(D) Analysis of the number of nuclei in vehicle- or 200 nM pregnenolone-treated mouse bone-marrow-derived OC cultures.

(E) Representative real-time images of Ctsk-Cre and mTmG bone marrow cells co-cultured in the presence of 20 ng/mL M-CSF and 20 ng/mL RANKL for 2 days and then in the presence of vehicle or 200 nM pregnenolone for the indicated time. Red color represents mononuclear cells; green fluorescence indicates fused OCs. Scale bars represent 20 µm.

Data are from 3–6 independent experiments, with error bars representing SD. *$p < 0.05$ and **$p < 0.01$; n.s., not significant.

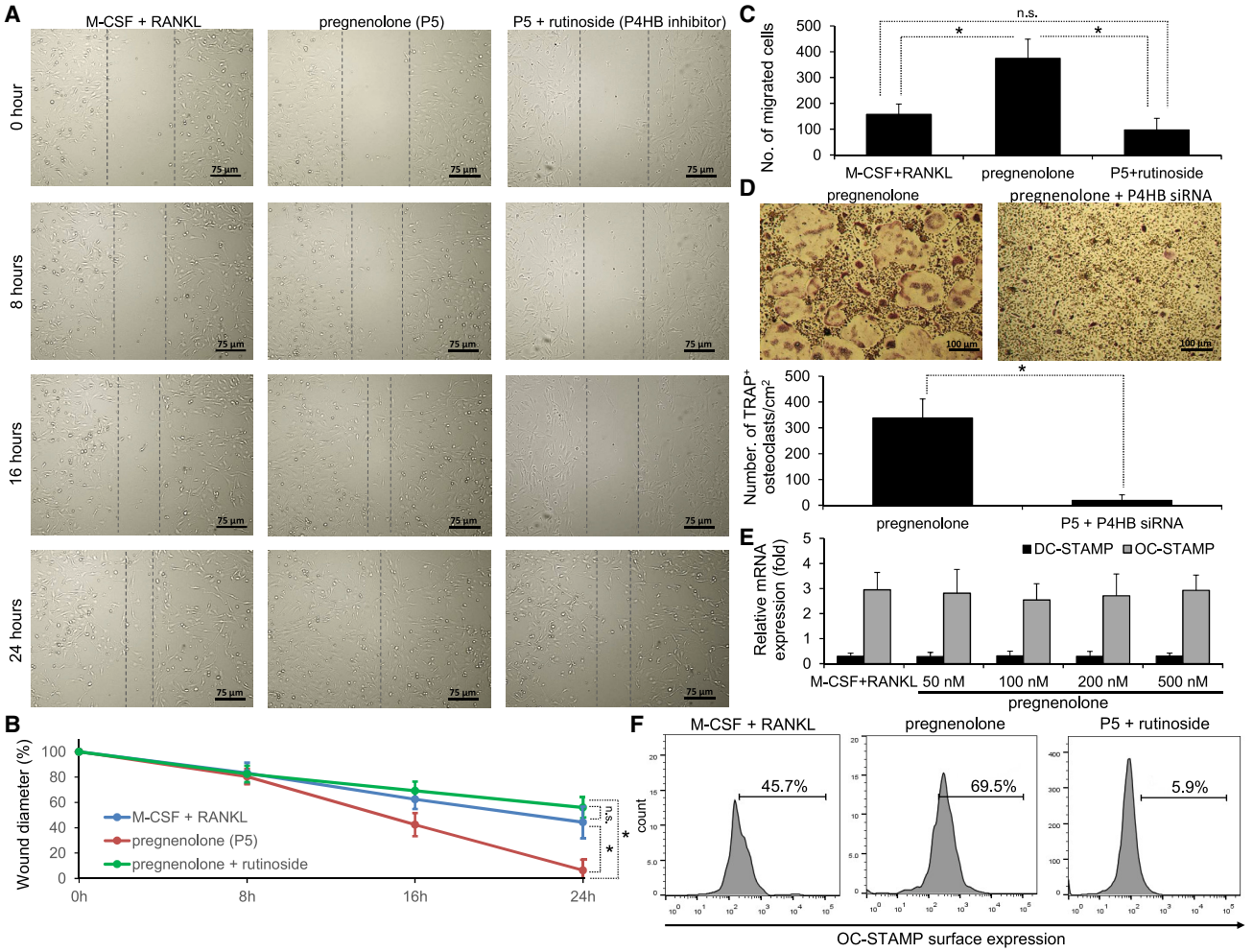

Figure 6. Pregnenolone promotes the migration and fusion of OC precursors via P4HB

(A and B) Representative images (A) and quantification (B) of wound closure by WT mouse bone-marrow-derived progenitors cultured in the presence of 20 ng/mL M-CSF and 20 ng/mL RANKL with or without 200 nM pregnenolone and with or without 3 μM quercetin-3-rutinoside for 24 h. Scale bars represent 75 μm.

(C) Quantification of Transwell migration by pre-OCs cultured in the presence of 20 ng/mL M-CSF and 20 ng/mL RANKL with or without 200 nM pregnenolone and with or without 3 μM quercetin-3-rutinoside.

(D) Representative images and quantification of TRAP-stained cell cultures of WT mouse bone-marrow-derived macrophages cultured in the presence of 200 nM pregnenolone with control (mock, left) or P4HB short hairpin RNA (shRNA) lentiviral particles (right). Scale bars represent 100 μm.

(E) Gene expression of *Tm7sf4* and *Ocstamp* genes (encoding for DC-STAMP and OC-STAMP, respectively) in WT mouse bone-marrow-derived progenitors cultured for 2 days in the presence of 20 and 20 ng/mL M-CSF and RANKL with or without the indicated concentration of pregnenolone for 3 days.

(F) Representative histograms of the binding of α-OC-STAMP antibody to WT bone marrow cells cultured for 2 days in the presence of 20 ng/mL M-CSF and RANKL with or without 200 nM pregnenolone and/or 3 μM quercetin-3-rutinoside.

Bar graphs show mean and SD of data from 3 experiments. *$p < 0.05$; n.s., not significant.

expressions of *Nfatc1* (encoding for NFATc1), *Acp5* (TRAP), *Calcr* (calcitonin receptor), *Itgb3* (integrin β_3-chain), *Tm7sf4* (DC-STAMP), and *Ctsk* (cathepsin K) were all strongly increased during osteoclast development (M-CSF and RANKL) but not during macrophage differentiation (M-CSF alone). On the other hand, administration of pregnenolone alone or after M-CSF and RANKL treatment did not alter the expression of those genes compared to the effects of M-CSF or M-CSF and RANKL, respectively (Figure 5A), indicating that solid-tumor-cell-derived pregnenolone is likely not sufficient alone for osteoclast-specific gene expression.

Pregnenolone promotes the fusion of osteoclast precursors

During the second phase of osteoclastogenesis, mononuclear osteoclast precursors fuse together to form the multinuclear polykarions. This intercellular fusion of pre-osteoclasts could be monitored in real time by a recently developed fluorescence-based osteoclast fusion assay.[22] This assay relies on red-to-green fluorescence conversion of the membrane-targeted tdTomato/EGFP (mTmG) transgene by Cre bacterial recombinase expressed under the control of osteoclast-specific cathepsin K promoter (Ctsk-Cre). Bone marrow precursors

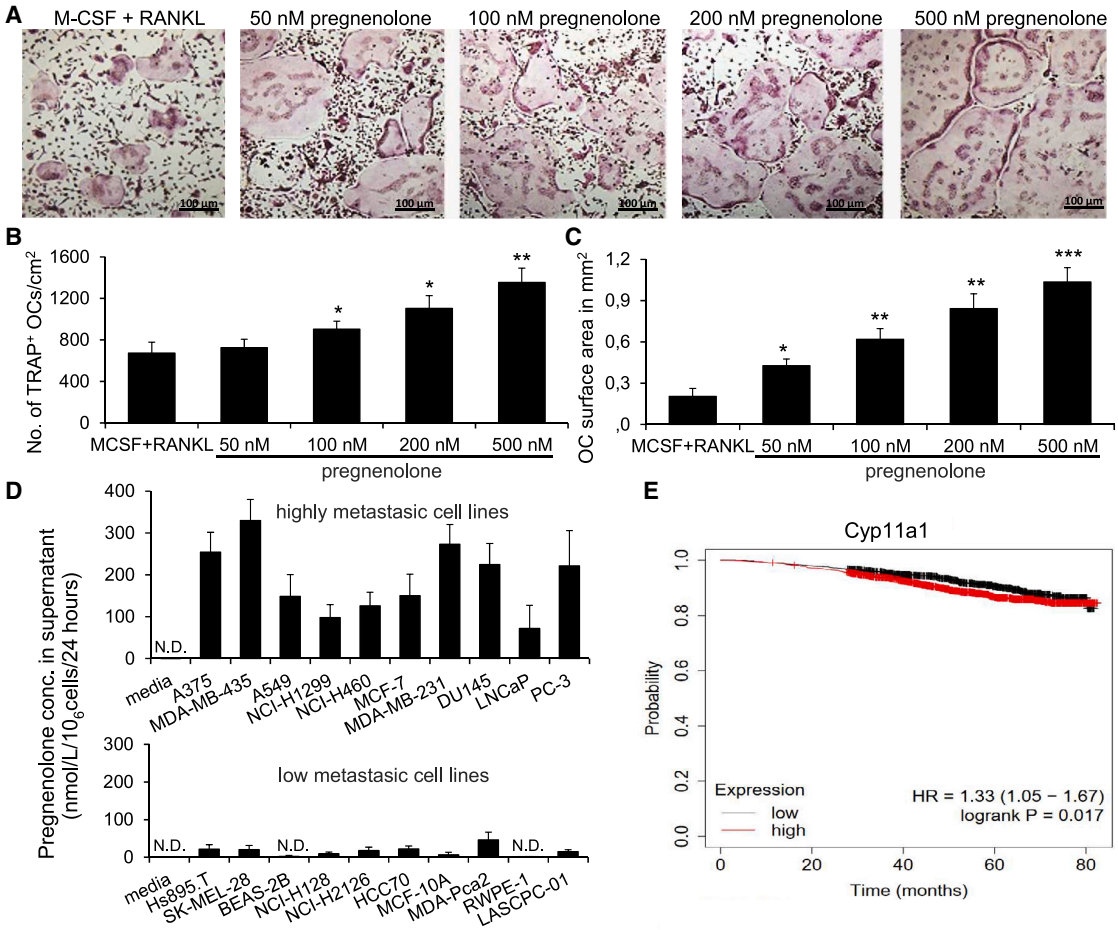

Figure 7. Pregnenolone promotes human osteoclastogenesis and is secreted by human tumor cells

(A–C) Representative images (A) and quantification (B and C) of TRAP-stained cell cultures of human blood mononuclear cell-derived OCs cultured for 2 days in the presence of 20 ng/mL recombinant human M-CSF and 20 ng/mL soluble human RANKL and then in the presence of the indicated concentration of pregnenolone or vehicle for 12 days. Scale bars represent 100 µm.

(D) Levels of pregnenolone in the supernatants of A375, MDA-MB-435S, A549, NCI-H1299, NCI-H460, MCF-7, MDA-MB-231, DU145, LNCaP, PC-3, Hs895.T, SK-MEL-28, BEAS-2B, NCI-H128, NCI-H2126, HCC70, MCF-10A, MDA-PCa-2b, RWPE-1, and LASCPC-01 cells measured by ELISA.

(E) Kaplan-Meier curve of breast-cancer-specific survival for 2,976 patients with high or low expression of *Cyp11a1* in the primary tumor.

Bar graphs show mean and SD of data from 3 independent experiments. *p < 0.05, **p < 0.01, and ***p < 0.002; n.s., not significant.

carrying the mTmG or the Ctsk-Cre transgene alone exhibit only red or no fluorescence, respectively. However, when mTmG and Ctsk-Cre progenitors are co-cultured under osteoclastogenic conditions, osteoclast-specific expression of Cre triggers removal of tdTomato and allows expression of EGFP within the fused osteoclast-like multinuclear cells. This red-to-green fluorescence conversion could be easily visualized and quantified.[22]

To test the effect of pregnenolone on osteoclast fusion, bone-marrow-derived progenitors were isolated from mTmG and Ctsk-Cre mice and co-cultured with or without 200 nM pregnenolone for 3 days after 2 day pre-treatment with physiological (20 and 20 ng/mL) or supra-physiological (50 and 50 ng/mL) concentrations of M-CSF and RANKL. As seen in Figures 5B and 5C in both conditions, the number of EGFP-positive cells significantly increased in the pregnenolone-treated cultures compared to the vehicle-treated ones. Further, there was a statistically significant increase in the number of nuclei within individual osteoclasts treated with pregnenolone compared to vehicle-treated cultures (Figure 5D). Real-time monitoring of osteoclast fusion in the presence or absence of pregnenolone confirmed that this effect takes places in less than 24 h (Figure 5E). These results indicate that tumor-derived pregnenolone promotes the development of osteoclasts by increasing the fusion of their precursors.

Pregnenolone promotes osteoclast fusion via P4HB

Next, we were interested in the mode of action of pregnenolone on osteoclasts at the molecular level. Recently, a proteome-wide spectrum of pregnenolone-binding proteins has been identified in an approach integrating chemical biology for probe synthesis with chemoproteomics.[23] Among pregnenolone interaction partners identified in this study and correlated with literature survey,

we recognized P4HB (also known as protein disulfide isomerase), an endoplasmic-reticulum-resident enzyme that catalyzes posttranslational disulfide bond formation and serves as a chaperone during protein folding. Since P4HB has also been implicated in macrophage migration,[24] and since the expression of P4HB was strongly upregulated during osteoclast differentiation (Figure S4A), we first tested the effect of pregnenolone on osteoclast precursor migration. As shown in Figures 6A and 6B, pregnenolone strongly promoted the migration of bone-marrow-derived pre-osteoclasts. However, quercetin-3-rutinoside, an inhibitor of P4HB,[25–28] blocked this effect of pregnenolone on pre-osteoclast migration in a wound-healing assay (Figures 6A and 6B). Further, Transwell migration of pre-osteoclast cells was also significantly enhanced by pregnenolone and strongly inhibited by quercetin-3-rutinoside (Figure 6C). Next, suppressing P4HB activity by using a short hairpin RNA technique in bone-marrow-precursor-derived osteoclasts grown in the presence of pregnenolone strongly suppressed osteoclastogenesis *in vitro* (Figures 6D, S4B, and S4C). The last question remained as to how P4HB, a protein disulfide isomerase localized in the endoplasmic reticulum, could regulate osteoclast fusion in a pregnenolone-dependent manner. To answer this question, we first compared the mRNA expression of osteoclast master fusogens *Tm7sf4* (encoding DC-STAMP) and *Ocstamp* (encoding OC-STAMP) in pre-osteoclasts upon M-CSF, RANKL and pregnenolone stimulation, but we could not detect any significant difference in the expression of the two genes (Figure 6E), which is in line with our previous observations that pregnenolone alone cannot induce osteoclast-specific gene expression (Figure 5A). However, when measuring the surface expression of OC-STAMP on pre-osteoclast by flow cytometry, we detected a strong increase upon pregnenolone stimulation compared to RANKL, which was almost completely abrogated by the inhibition of P4HB with quercetin-3-rutinoside (Figure 6F). Accordingly, we believe that P4HB is able to regulate the posttranslational protein levels and surface expression of master fusogen OC-STAMP in osteoclast precursors and that pregnenolone stimulates it. To test the role of P4HB in osteoclasts *in vivo*, 10 mg/kg quercetin-3-rutinoside was administered orally to the mice injected with E0771/bone cells into the caudal artery. Importantly, P4HB inhibitor quercetin-3-rutinoside significantly inhibited bone metastasis formation in the animals (Figure S4D). Further, intravenous injections of WT osteoclast precursors into *Rank*$^{-/-}$ neonates at postnatal days 5, 7, and 9 resulted in partial rescue of long-bone development as assessed by micro-CT scans using the method described by Jacome-Galarza et al.,[29] while *P4hb*$^{-/-}$ precursors were not able to rescue bone development in *Rank*$^{-/-}$ infants (Figure S4E). Abrogation of P4HB activity abolished the capacity of the transfused osteoclast precursors to decrease bone volume/total volume (BV/TV) ratio and increase osteoclast numbers in the histological sections of the femurs of the animals (Figure S4F). Collectively, these data suggest that P4HB plays an important role in osteoclasts *in vivo* and that administration of WT, but not *P4hb*$^{-/-}$, osteoclast precursors can rescue bone development in *Rank*$^{-/-}$ mice; however, future experiments are required to better understand the role of P4HB in *in vivo* bone homeostasis, e.g., by using *P4hb*$^{-/-}$ mice.[30]

Taken together, these results indicate we implicated P4HB in osteoclasts as a potential interaction partner of tumor-cell-derived *pregnenolone* and found that this molecule can drive pre-osteoclast cell migration and fusion as well as *in vitro* and *in vivo* development of osteoclasts.

Pregnenolone promotes human osteoclastogenesis and is secreted by human tumor cells

Finally, we were interested in whether the same mechanism works in human bone tumors. To test whether pregnenolone can promote not only murine but also human osteoclastogenesis, peripheral blood mononuclear cells of healthy volunteers were differentiated into osteoclasts in the presence of pregnenolone or vehicle after pre-treatment with M-CSF and RANKL. As shown in Figures 7A–7C, pregnenolone dose-dependently increased the number and size of osteoclasts compared to the control. Moreover, we were able to detect pregnenolone secreted in the nanomolar concentration range in the supernatants of highly bone-metastatic A375 and MDA-MB-435S melanoma; A549, NCI-H1299, and NCI-H460 lung; MCF-7 and MDA-MB-231 breast; and DU145, LNCaP, and PC-3 prostate cancer cells but not in the supernatants of non-metastatic or low-bone-metastatic Hs895.T and SK-MEL-28 melanoma; BEAS-2B, NCI-H128, and NCI-H2126 lung; HCC70 and MCF-10A breast; or MDA-PCa-2b, RWPE-1, and LASCPC-01 prostate cell lines (Figure 7D). These results indicate that osteotropic human cancer cell lines can also produce pregnenolone, which promotes not only murine but human osteoclastogenesis as well. Further, in a cohort of 2,976 people with breast cancer,[31] higher expression of *Cyp11a1* was found to be associated with worst prognosis (Figure 7E); however, future studies are required to better understand the role of CYP11A1 in human bone tumors.

DISCUSSION

Osteolytic bone metastasis formation is a multistep process, which requires complex interplay between tumor cells and osteoclasts, and it is regulated by microenvironmental factors.[32] Here, we describe a potential regulator of osteoclastogenesis secreted by solid cancer cells. Based on our results, *de novo* production of the steroid pregnenolone by tumor cells in a CYP11A1-enzyme-dependent manner drives osteoclastogenesis and osteolytic skeletal lesion formation (Figure 1). CRISPR-Cas9-mediated deletion of the gene encoding CYP11A1 in the tumor cells protects mice from bone metastases (Figure 2) and cancer-cell-induced, osteoclast-mediated osteolysis (Figure 3). Further, administration of pregnenolone promotes the development and function of osteoclasts *in vitro* (Figure 4). Sun et al. recently reported that high levels of pregnenolone in the μM concentration range can exert an inhibitory effect on osteoclastogenesis,[33] which is in line with our own observations (Figure 4). However, we believe that tumor-derived steroids do not reach such high concentrations within the tumor microenvironment to induce the apoptosis of osteoclast-lineage cells. Instead, we think that pregnenolone secreted in the nM concentration range by the osteotropic tumor cells strongly promotes osteoclast development and function (Figure 4).

Next, we investigated the mechanism of action of pregnenolone on osteoclasts. The potential mechanism of how tumor-derived pregnenolone promotes osteoclastogenesis is likely via the enhancement of the osteoclast fusion machinery (Figure 5). As the early steps of intercellular fusion occur, osteoclast precursors migrate toward each other. During this process, P4HB, a molecule known to interact with pregnenolone,[23] can drive pre-osteoclast cell migration, based on our results (Figure 6). Moreover, we also found that pregnenolone via P4HB is capable of regulating the surface expression of OC-STAMP, a molecule critical for osteoclast fusion (Figure 6). Interestingly, a recent integrated proteomics and network analysis study implicated P4HB as a candidate gene involved in osteoporosis,[34] another disease characterized by excessive osteoclast activity. Further, there could be more interaction partners of pregnenolone in osteoclasts. Part of the identified pregnenolone interactome in the chemoproteomics assay is related to steroid transport across the cell.[23] Voltage-dependent anion channels, VDAC1–VDAC3, are important regulators of metabolite exchange between mitochondria and the rest of the cell. All three VDACs were retrieved in the study by Roy et al.,[23] and based on our results (Figures S4A) and a recent paper,[35] an anti-VDAC1 antibody can abrogate osteoclastogenesis and osteoclast-mediated bone resorption as well (Figures S4G–S4I). Finally, we demonstrated that osteotropic human cancer cell lines can also produce pregnenolone, which promotes not only murine but also human osteoclastogenesis and disease progression in patients with breast cancer (Figure 7).

RANKL is essential for the induction of osteoclastogenesis in humans and mice.[36] Loss or mutation of RANKL or its receptor on osteoclasts, RANK, results in osteopetrosis in both species because of a complete lack of osteoclasts.[37] Further, it has also been described that certain tumor cells can express RANKL themselves to promote osteoclast development and function.[38–40] However, to date, no other molecule has been proven capable of inducing osteoclast development independently of RANKL.[41] Recent studies identified certain tumor-cell-derived soluble factors as potential regulators of osteoclastogenesis, but they failed to induce osteoclast differentiation and osteolytic bone metastasis formation in further experiments.[42] While other factors were also implicated to be able to induce RANKL-independent osteoclast differentiation, they might not be able to promote osteoclastogenesis alone and substitute for the RANK ligand completely.[41] Accordingly, we believe that tumor-derived pregnenolone promotes osteoclastogenesis synergistically in combination with RANKL and M-CSF. Besides producing pregnenolone, cancer cells can secrete both M-CSF and PTHrP—which in turn increases RANKL expression on osteoblasts—and together with pregnenolone, they stimulate osteoclast development and fusion via P4HB.

Taken together, our results demonstrate that *Cyp11a1*-expressing malignant tumors *de novo* produce the steroid pregnenolone, which is capable of driving the development of bone metastases by promoting osteoclastogenesis. In addition to its role outside the adrenals, gonads, and placenta, CYP11A1-driven extraglandular steroidogenesis has recently been implicated within the non-transformed tumor microenvironment, where cancer cells can subvert immune cell function to evade immune responses.[18–21] Accordingly, pharmacological interference with local steroidogenesis in osteolytic skeletal lesions may result in parallel inhibition of pro-tumorigenic immune cell subsets and bone-resorbing osteoclasts. In a broader context, better understanding of the molecular and cellular mechanisms of local steroidogenesis within malignant tumors may drive the development of novel therapeutic interventions for patients with metastatic disease.

Limitations of the study

There may be potential limitations of this study. The generation of CRISPR-Cas9-engineered cell lines may result in undesired phenotypes caused by potential off-target genetic alterations. Further application of the generated cell lines will require comprehensive DNA sequencing to avoid introducing unintended DNA changes that could result in oncogenic transformation or off-target phenotypes. Future work is also required to better understand the role of CYP11A1 and P4HB in human bone tumors and during physiological and pathological bone turnover.

STAR★METHODS

Detailed methods are provided in the online version of this paper and include the following:

- KEY RESOURCES TABLE
- RESOURCE AVAILABILITY
  - Lead contact
  - Materials availability
  - Data and code availability
- EXPERIMENTAL MODEL AND STUDY PARTICIPANT DETAILS
  - Clinical samples
  - Animals
  - Cell lines
- METHOD DETAILS
  - Deletion and overexpression of the genes encoding CYP11A1 and P4HB
  - Tumor models
  - Micro-CT and histomorphometric analyses
  - *In vitro* and *in vivo* mouse macrophage and osteoclast cultures and resorption assays
  - Detection of cell survival and OC-STAMP surface expression
  - Actin ring formation assay
  - *In vitro* osteoclast fusion assay
  - RNA sequencing and quantitative PCR
  - *In vitro* wound healing and migration assays
  - Steroid measurement by liquid chromatography mass spectrometry (LC-MS/MS)
  - Immunoblotting and ELISA
- QUANTIFICATION AND STATISTICAL ANALYSIS

SUPPLEMENTAL INFORMATION

Supplemental information can be found online at https://doi.org/10.1016/j.celrep.2024.113936.

ACKNOWLEDGMENTS

We thank Simon P. Nagy and Thomas C. Champion for expert technical assistance, Michael Sixt for the Lifeact-EGFP and Shigeaki Kato for the Ctsk-Cre transgenic mice, Klaus Okkenhaug for the LLC and MC38 cells, Gabor Kovacs and Zoltan Jakus for help with histomorphometry, and Attila Mocsai for critical experimental tools and advice. LC-MS/MS data were obtained at the University of Edinburgh, Edinburgh Clinical Research Facility, Mass Spectrometry Core (RRID: SCR_021833), using the AB SCIEX QTRAP 6500 plus system (RRID: SCR_021831). We acknowledge Scott Denham for maintenance of the LC-MS/MS instrumentation and liquid handling robotics. This work was supported by the Hungarian National Scientific Research Fund (NKFIH-OTKA grant no. FK132971 to D.S.G.), the Semmelweis University Scientific and Research Innovation Fund (STIA_18 to D.S.G.), the Hungarian National, Development & Innovation Office's TKP Fund (SEMTHREUM grant to D.S.G.), the Janos Bolyai Research Scholarship of the Hungarian Academy of Sciences (BO/00359/22 to D.S.G.), and the new National Excellence Program of the Ministry for Culture and Innovation (UNKP-23-5 to D.S.G.). B.M. is supported by CRUK Career Development Fellowship (RCCFEL\100095), NSF-BIO/UKRI-BBSRC project grant (BB/V006126/1), and MRC project grant (MR/V028995/1).

AUTHOR CONTRIBUTIONS

L.F.S., J.B.H., and P.B. performed most of the experiments and analyzed and interpreted the data. T.H. provided critical experimental tools (E0771/bone cells). C.D.-N. conducted micro-CT experiments. S.P. performed RNA sequencing analysis. B.M. provided advice on CYP11A1. J.P.S. and N.Z.M.H. conducted LC-MS/MS-based steroid measurements. D.S.G. designed experiments, analyzed and interpreted the data, supervised the project, and wrote the manuscript.

DECLARATION OF INTERESTS

The authors declare no competing interests.

Received: July 21, 2023
Revised: November 8, 2023
Accepted: February 23, 2024

REFERENCES

1. Mundy, G.R. (2002). Metastasis: metastasis to bone: causes, consequences and therapeutic opportunities. Nat. Rev. Cancer *2*, 584–593. https://doi.org/10.1038/nrc867.
2. Weilbaecher, K.N., Guise, T.A., and McCauley, L.K. (2011). Cancer to bone: a fatal attraction. Nat. Rev. Cancer *11*, 411–425. https://doi.org/10.1038/nrc3055.
3. Croucher, P.I., McDonald, M.M., and Martin, T.J. (2016). Bone metastasis: the importance of the neighbourhood. Nat. Rev. Cancer *16*, 373–386. https://doi.org/10.1038/nrc.2016.44.
4. Coleman, R.E., and Rubens, R.D. (1987). The clinical course of bone metastases from breast cancer. Br. J. Cancer *55*, 61–66. https://doi.org/10.1038/bjc.1987.13.
5. Faccio, R. (2011). Immune regulation of the tumor/bone vicious cycle. Ann. N. Y. Acad. Sci. *1237*, 71–78. https://doi.org/10.1111/j.1749-6632.2011.06244.x.
6. Boyle, W.J., Simonet, W.S., and Lacey, D.L. (2003). Osteoclast differentiation and activation. Nature *423*, 337–342. https://doi.org/10.1038/nature01658.
7. Takayanagi, H. (2010). New immune connections in osteoclast formation. Ann. N. Y. Acad. Sci. *1192*, 117–123. https://doi.org/10.1111/j.1749-6632.2009.05303.x.
8. Gyori, D., and Mocsai, A. (2016). Osteoclasts in Inflammation. In Compendium of Inflammatory Diseases, M.J. Parnham, ed. (Springer). https://doi.org/10.1007/978-3-7643-8550-7_155.
9. Teitelbaum, S.L. (2000). Bone resorption by osteoclasts. Science *289*, 1504–1508. https://doi.org/10.1126/science.289.5484.1504.
10. Thomas, R.J., Guise, T.A., Yin, J.J., Elliott, J., Horwood, N.J., Martin, T.J., and Gillespie, M.T. (1999). Breast cancer cells interact with osteoblasts to support osteoclast formation. Endocrinology *140*, 4451–4458. https://doi.org/10.1210/endo.140.10.7037.
11. Suva, L.J., Winslow, G.A., Wettenhall, R.E., Hammonds, R.G., Moseley, J.M., Diefenbach-Jagger, H., Rodda, C.P., Kemp, B.E., Rodriguez, H., and Chen, E.Y. (1987). A parathyroid hormone-related protein implicated in malignant hypercalcemia: cloning and expression. Science *237*, 893–896. https://doi.org/10.1126/science.3616618.
12. Hiraga, T., and Ninomiya, T. (2019). Establishment and characterization of a C57BL/6 mouse model of bone metastasis of breast cancer. J. Bone Miner. Metab. *37*, 235–242. https://doi.org/10.1007/s00774-018-0927-y.
13. Belelli, D., and Lambert, J.J. (2005). Neurosteroids: endogenous regulators of the GABA(A) receptor. Nat. Rev. Neurosci. *6*, 565–575. https://doi.org/10.1038/nrn1703.
14. Slominski, A., Zbytek, B., Nikolakis, G., Manna, P.R., Skobowiat, C., Zmijewski, M., Li, W., Janjetovic, Z., Postlethwaite, A., Zouboulis, C.C., and Tuckey, R.C. (2013). Steroidogenesis in the skin: implications for local immune functions. J. Steroid Biochem. Mol. Biol. *137*, 107–123. https://doi.org/10.1016/j.jsbmb.2013.02.006.
15. Vacchio, M.S., Papadopoulos, V., and Ashwell, J.D. (1994). Steroid production in the thymus: implications for thymocyte selection. J. Exp. Med. *179*, 1835–1846. https://doi.org/10.1084/jem.179.6.1835.
16. Cima, I., Corazza, N., Dick, B., Fuhrer, A., Herren, S., Jakob, S., Ayuni, E., Mueller, C., and Brunner, T. (2004). Intestinal epithelial cells synthesize glucocorticoids and regulate T cell activation. J. Exp. Med. *200*, 1635–1646. https://doi.org/10.1084/jem.20031958.
17. Hostettler, N., Bianchi, P., Gennari-Moser, C., Kassahn, D., Schoonjans, K., Corazza, N., and Brunner, T. (2012). Local glucocorticoid production in the mouse lung is induced by immune cell stimulation. Allergy *67*, 227–234. https://doi.org/10.1111/j.1398-9995.2011.02749.x.
18. Mahata, B., Zhang, X., Kolodziejczyk, A.A., Proserpio, V., Haim-Vilmovsky, L., Taylor, A.E., Hebenstreit, D., Dingler, F.A., Moignard, V., Göttgens, B., et al. (2014). Single-cell RNA sequencing reveals T helper cells synthesizing steroids de novo to contribute to immune homeostasis. Cell Rep. *7*, 1130–1142. https://doi.org/10.1016/j.celrep.2014.04.011.
19. Mahata, B., Pramanik, J., van der Weyden, L., Polanski, K., Kar, G., Riedel, A., Chen, X., Fonseca, N.A., Kundu, K., Campos, L.S., et al. (2020). Tumors induce de novo steroid biosynthesis in T cells to evade immunity. Nat. Commun. *11*, 3588. https://doi.org/10.1038/s41467-020-17339-6.
20. Chakraborty, S., Pramanik, J., and Mahata, B. (2021). Revisiting steroidogenesis and its role in immune regulation with the advanced tools and technologies. Genes Immun. *22*, 125–140. https://doi.org/10.1038/s41435-021-00139-3.
21. Slominski, A.T., Mahata, B., Raman, C., and Bereshchenko, O. (2021). Editorial: Steroids and Secosteroids in the Modulation of Inflammation and Immunity. Front. Immunol. *12*, 825577. https://doi.org/10.3389/fimmu.2021.825577.
22. Pánczél, Á., Nagy, S.P., Farkas, J., Jakus, Z., Győri, D.S., and Mócsai, A. (2021). Fluorescence-Based Real-Time Analysis of Osteoclast Development. Front. Cell Dev. Biol. *9*, 657935. https://doi.org/10.3389/fcell.2021.657935.
23. Roy, S., Sipthorp, J., Mahata, B., Pramanik, J., Hennrich, M.L., Gavin, A.C., Ley, S.V., and Teichmann, S.A. (2021). CLICK-enabled analogues reveal pregnenolone interactomes in cancer and immune cells. iScience *24*, 102485. https://doi.org/10.1016/j.isci.2021.102485.
24. Xiao, Y., Li, C., Gu, M., Wang, H., Chen, W., Luo, G., Yang, G., Zhang, Z., Zhang, Y., Xian, G., et al. (2018). Protein Disulfide Isomerase Silence

Inhibits Inflammatory Functions of Macrophages by Suppressing Reactive Oxygen Species and NF-κB Pathway. Inflammation *41*, 614–625. https://doi.org/10.1007/s10753-017-0717-z.

25. Jasuja, R., Passam, F.H., Kennedy, D.R., Kim, S.H., van Hessem, L., Lin, L., Bowley, S.R., Joshi, S.S., Dilks, J.R., Furie, B., et al. (2012). Protein disulfide isomerase inhibitors constitute a new class of antithrombotic agents. J. Clin. Invest. *122*, 2104–2113. https://doi.org/10.1172/JCI61228.

26. Lin, L., Gopal, S., Sharda, A., Passam, F., Bowley, S.R., Stopa, J., Xue, G., Yuan, C., Furie, B.C., Flaumenhaft, R., et al. (2015). Quercetin-3-rutinoside Inhibits Protein Disulfide Isomerase by Binding to Its b'x Domain. J. Biol. Chem. *290*, 23543–23552. https://doi.org/10.1074/jbc.M115.666180.

27. Stopa, J.D., Neuberg, D., Puligandla, M., Furie, B., Flaumenhaft, R., and Zwicker, J.I. (2017). Protein disulfide isomerase inhibition blocks thrombin generation in humans by interfering with platelet factor V activation. JCI Insight *2*, e89373. https://doi.org/10.1172/jci.insight.89373.

28. Zwicker, J.I., Schlechter, B.L., Stopa, J.D., Liebman, H.A., Aggarwal, A., Puligandla, M., Caughey, T., Bauer, K.A., Kuemmerle, N., Wong, E., et al. (2019). Targeting protein disulfide isomerase with the flavonoid isoquercetin to improve hypercoagulability in advanced cancer. JCI Insight *4*, e125851. https://doi.org/10.1172/jci.insight.125851.

29. Jacome-Galarza, C.E., Percin, G.I., Muller, J.T., Mass, E., Lazarov, T., Eitler, J., Rauner, M., Yadav, V.K., Crozet, L., Bohm, M., et al. (2019). Developmental origin, functional maintenance and genetic rescue of osteoclasts. Nature *568*, 541–545. https://doi.org/10.1038/s41586-019-1105-7.

30. Hahm, E., Li, J., Kim, K., Huh, S., Rogelj, S., and Cho, J. (2013). Extracellular protein disulfide isomerase regulates ligand-binding activity of αMβ2 integrin and neutrophil recruitment during vascular inflammation. Blood *121*, 3789–3800. https://doi.org/10.1182/blood-2012-11-467985.

31. Győrffy, B. (2021). Survival analysis across the entire transcriptome identifies biomarkers with the highest prognostic power in breast cancer. Comput. Struct. Biotechnol. J. *19*, 4101–4109. https://doi.org/10.1016/j.csbj.2021.07.014.

32. Győri, D.S., and Mócsai, A. (2020). Osteoclast Signal Transduction During Bone Metastasis Formation. Front. Cell Dev. Biol. *8*, 507. https://doi.org/10.3389/fcell.2020.00507.

33. Sun, X., Zhang, C., Guo, H., Chen, J., Tao, Y., Wang, F., Lin, X., Liu, Q., Su, L., and Qin, A. (2020). Pregnenolone Inhibits Osteoclast Differentiation and Protects Against Lipopolysaccharide-Induced Inflammatory Bone Destruction and Ovariectomy-Induced Bone Loss. Front. Pharmacol. *11*, 360. https://doi.org/10.3389/fphar.2020.00360.

34. Zeng, Y., Zhang, L., Zhu, W., He, H., Sheng, H., Tian, Q., Deng, F.Y., Zhang, L.S., Hu, H.G., and Deng, H.W. (2017). Network based subcellular proteomics in monocyte membrane revealed novel candidate genes involved in osteoporosis. Osteoporos. Int. *28*, 3033–3042. https://doi.org/10.1007/s00198-017-4146-5.

35. Kotake, S., Yago, T., Kawamoto, M., and Nanke, Y. (2013). Voltage-dependent anion channels (VDACs, porin) expressed in the plasma membrane regulate the differentiation and function of human osteoclasts. Cell Biol. Int. *37*, 65–77. https://doi.org/10.1002/cbin.10013.

36. Kong, Y.Y., Yoshida, H., Sarosi, I., Tan, H.L., Timms, E., Capparelli, C., Morony, S., Oliveira-dos-Santos, A.J., Van, G., Itie, A., et al. (1999). OPGL is a key regulator of osteoclastogenesis, lymphocyte development and lymph-node organogenesis. Nature *397*, 315–323. https://doi.org/10.1038/16852.

37. Takayanagi, H. (2007). Osteoimmunology: shared mechanisms and crosstalk between the immune and bone systems. Nat. Rev. Immunol. *7*, 292–304. https://doi.org/10.1038/nri2062.

38. Brown, J.M., Corey, E., Lee, Z.D., True, L.D., Yun, T.J., Tondravi, M., and Vessella, R.L. (2001). Osteoprotegerin and rank ligand expression in prostate cancer. Urology *57*, 611–616. https://doi.org/10.1016/s0090-4295(00)01122-5.

39. Sezer, O., Heider, U., Zavrski, I., Kühne, C.A., and Hofbauer, L.C. (2003). RANK ligand and osteoprotegerin in myeloma bone disease. Blood *101*, 2094–2098. https://doi.org/10.1182/blood-2002-09-2684.

40. Farrugia, A.N., Atkins, G.J., To, L.B., Pan, B., Horvath, N., Kostakis, P., Findlay, D.M., Bardy, P., and Zannettino, A.C.W. (2003). Receptor activator of nuclear factor-kappaB ligand expression by human myeloma cells mediates osteoclast formation in vitro and correlates with bone destruction in vivo. Cancer Res. *63*, 5438–5445.

41. Tanaka, S. (2017). RANKL-Independent Osteoclastogenesis: A Long-Standing Controversy. J. Bone Miner. Res. *32*, 431–433. https://doi.org/10.1002/jbmr.3092.

42. Tsukasaki, M., Hamada, K., Okamoto, K., Nagashima, K., Terashima, A., Komatsu, N., Win, S.J., Okamura, T., Nitta, T., Yasuda, H., et al. (2017). LOX Fails to Substitute for RANKL in Osteoclastogenesis. J. Bone Miner. Res. *32*, 434–439. https://doi.org/10.1002/jbmr.2990.

43. Ran, F., Hsu, P., and Wright, J. (2013). Genome engineering using the CRISPR-Cas9 system. Nat. Protoc. *8*, 2281–2308. https://doi.org/10.1038/nprot.2013.143.

44. Sanjana, N., Shalem, O., and Zhang, F. (2014). Improved vectors and genome-wide libraries for CRISPR screening. Nat Methods *11*, 783–784. https://doi.org/10.1038/nmeth.3047.

45. Riedl, J., Flynn, K.C., Raducanu, A., Gärtner, F., Beck, G., Bösl, M., Bradke, F., Massberg, S., Aszodi, A., Sixt, M., and Wedlich-Söldner, R. (2010). Lifeact mice for studying F-actin dynamics. Nat. Methods *7*, 168–169. https://doi.org/10.1038/nmeth0310-168.

46. Nakamura, T., Imai, Y., Matsumoto, T., Sato, S., Takeuchi, K., Igarashi, K., Harada, Y., Azuma, Y., Krust, A., Yamamoto, Y., et al. (2007). Estrogen prevents bone loss via estrogen receptor α and induction of Fas ligand in osteoclasts. Cell *130*, 811–823. https://doi.org/10.1016/j.cell.2007.07.025.

47. Muzumdar, M.D., Tasic, B., Miyamichi, K., Li, L., and Luo, L. (2007). A global double-fluorescent Cre reporter mouse. Genesis *45*, 593–605. https://doi.org/10.1002/dvg.20335.

48. Hanada, R., Leibbrandt, A., Hanada, T., Kitaoka, S., Furuyashiki, T., Fujihara, H., Trichereau, J., Paolino, M., Qadri, F., Plehm, R., et al. (2009). Central control of fever and female body temperature by RANKL/RANK. Nature *462*, 505–509. https://doi.org/10.1038/nature08596.

49. Montague, T.G., Cruz, J.M., Gagnon, J.A., Church, G.M., and Valen, E. (2014). CHOPCHOP: a CRISPR/Cas9 and TALEN web tool for genome editing. Nucleic Acids Res. *42*, W401–W407. https://doi.org/10.1093/nar/gku410.

50. Gyori, D., Lim, E.L., Grant, F.M., Spensberger, D., Roychoudhuri, R., Shuttleworth, S.J., Okkenhaug, K., Stephens, L.R., and Hawkins, P.T. (2018). Compensation between CSF1R+ macrophages and FOXP3+ Treg cells drives resistance to tumor immunotherapy. JCI Insight *3*, e120631. https://doi.org/10.1172/jci.insight.120631.

51. Lim, E.L., Cugliandolo, F.M., Rosner, D.R., Gyori, D., Roychoudhuri, R., and Okkenhaug, K. (2018). Phosphoinositide 3-kinase δ inhibition promotes antitumor responses but antagonizes checkpoint inhibitors. JCI Insight *3*, e120626. https://doi.org/10.1172/jci.insight.120626.

52. Kuchimaru, T., Kataoka, N., Nakagawa, K., Isozaki, T., Miyabara, H., Minegishi, M., Kadonosono, T., and Kizaka-Kondoh, S. (2018). A reliable murine model of bone metastasis by injecting cancer cells through caudal arteries. Nat. Commun. *9*, 2981. https://doi.org/10.1038/s41467-018-05366-3.

53. Kertész, Z., Gyori, D., Körmendi, S., Fekete, T., Kis-Tóth, K., Jakus, Z., Schett, G., Rajnavölgyi, E., Dobó-Nagy, C., and Mócsai, A. (2012). Phospholipase Cγ2 is required for basal but not oestrogen deficiency-induced bone resorption. Eur. J. Clin. Invest. *42*, 49–60. https://doi.org/10.1111/j.1365-2362.2011.02556.x.

54. Győri, D., Csete, D., Benkő, S., Kulkarni, S., Mandl, P., Dobó-Nagy, C., Vanhaesebroeck, B., Stephens, L., Hawkins, P.T., and Mócsai, A. (2014). The phosphoinositide 3-kinase isoform PI3Kβ regulates

osteoclast-mediated bone resorption in humans and mice. Arthritis Rheumatol. *66*, 2210–2221. https://doi.org/10.1002/art.38660.

55. Csete, D., Simon, E., Alatshan, A., Aradi, P., Dobó-Nagy, C., Jakus, Z., Benkő, S., Győri, D.S., and Mócsai, A. (2019). Hematopoietic or Osteoclast-Specific Deletion of Syk Leads to Increased Bone Mass in Experimental Mice. Front. Immunol. *10*, 937. https://doi.org/10.3389/fimmu.2019.00937.
56. Dempster, D.W., Compston, J.E., Drezner, M.K., Glorieux, F.H., Kanis, J.A., Malluche, H., Meunier, P.J., Ott, S.M., Recker, R.R., and Parfitt, A.M. (2013). Standardized nomenclature, symbols, and units for bone histomorphometry: a 2012 update of the report of the ASBMR Histomorphometry Committee. J. Bone Miner. Res. *28*, 2–17. https://doi.org/10.1002/jbmr.1805.
57. Kiss, M., Czimmerer, Z., Nagy, G., Bieniasz-Krzywiec, P., Ehling, M., Pap, A., Poliska, S., Boto, P., Tzerpos, P., Horvath, A., et al. (2017). Retinoid X receptor suppresses a metastasis-promoting transcriptional program in myeloid cells via a ligand-insensitive mechanism. Proc. Natl. Acad. Sci. USA *114*, 10725–10730. https://doi.org/10.1073/pnas.1700785114.
58. Orosz, A., Walzog, B., and Mócsai, A. (2021). In Vivo Functions of Mouse Neutrophils Derived from HoxB8-Transduced Conditionally Immortalized Myeloid Progenitors. J. Immunol. *206*, 432–445. https://doi.org/10.4049/jimmunol.2000807.
59. Gregory, S., Denham, S.G., Lee, P., Simpson, J.P., and Homer, N.Z.M. (2023). Using LC-MS/MS to Determine Salivary Steroid Reference Intervals in a European Older Adult Population. Metabolites *13*, 265. https://doi.org/10.3390/metabo13020265.
60. Mócsai, A., Zhou, M., Meng, F., Tybulewicz, V.L., and Lowell, C.A. (2002). Syk is required for integrin signaling in neutrophils. Immunity *16*, 547–558. https://doi.org/10.1016/s1074-7613(02)00303-5.

STAR★METHODS

KEY RESOURCES TABLE

REAGENT or RESOURCE	SOURCE	IDENTIFIER
Antibodies		
CYP11A1 antibody	Abcam	Cat# ab175408; RRID:AB_2721042
P4HB antibody	Abcam	Cat# ab2792; RRID:AB_303304
VDAC1/Porin antibody	Santa Cruz BioTech.	Cat# sc-58649; RRID:AB_632587
mouse monoclonal IgG2b antibody	Santa Cruz BioTech.	Cat# sc-3879; RRID:AB_737262
FITC-labeled anti-OC-STAMP-mAb	Novus Biologicals	Cat# NBP1-78156; RRID:AB_11038923
β-actin antibody	Merck/Sigma	Cat# clone AC-74; RRID:AB_476743
HRP-labeled anti-rabbit IgG antibody	GE Healthcare	Cat# RPN4301; RRID:AB_2650489
HRP-labeled anti-mouse IgG antibody	GE Healthcare	Cat# NA931; RRID:AB_772210
Bacterial and virus strains		
P4HB shRNA lentiviral particles	Santa Cruz BioTech.	Cat# sc-36202
Biological samples		
BMDM from mouse bone marrow	This paper	N/A
mice tumor tissues	This paper	N/A
human blood-derived monocytes	Semmelweis University	N/A
Chemicals, peptides, and recombinant proteins		
recombinant murine M-CSF	PeproTech	Cat# 315-02
recombinant murine soluble RANKL	PeproTech	Cat# 315-11
recombinant human M-CSF	PeproTech	Cat# 300-25
recombinant human soluble RANKL	PeproTech	Cat# 310-01
pregnenolone	Merck/Sigma	Cat# P-104
aminogluthetimide	Merck/Sigma	Cat# A0496000
quercetin-3-rutinoside	Merck/Sigma	Cat# PHL83535
Lipofectamine 3000	Thermo-Fisher Scientific	Cat# L3000015
OSTEOSOFT	Merck/Sigma	Cat# 101728
7-amino-actinomycin	BD Pharmingen	Cat# 559925
DAPI	Invitrogen	Cat# D1306
FBS	Gibco	Cat# 26140079
PMSF	Merck/Sigma	Cat# PMSF-RO
aprotinin	Merck/Sigma	Cat# ROAPRO
phosphatase inhibitor cocktail 1	Merck/Sigma	Cat# P8340
phosphatase inhibitor cocktail 2	Merck/Sigma	Cat# P5726
DMSO	Merck/Sigma	Cat# 5.89569
sodium-orthovanadate	Merck/Sigma	Cat# 567540-5GM
ECL	GE Healthcare	Cat# 28980926
trypsin-EDTA	Merck/Sigma	Cat# T4049
puromycin	Thermo-Fisher Scientific	Cat# AAJ67236XF
G418	Thermo-Fisher Scientific	Cat# 10131035
Ficoll-Paque	GE Healthcare	Cat# 17-1440-03
Dulbecco's Modified Eagle Medium (DMEM)	Thermo-Fisher Scientific	Cat# 11965084
α-Minimum Essential Medium Eagle (αMEM)	Thermo-Fisher Scientific	Cat# 12571063
Bone slices	Immunodiagnostic Syst.	Cat# DT-1BON1000-96
BioCoat Osteologic slides	BD Pharmingen	Cat# 2267
Critical commercial assays		
TRAP staining kit	Merck/Sigma	Cat# 387A
PE Annexin V Apoptosis Detection Kit	BD Pharmingen	Cat# AB_2869265

(*Continued on next page*)

Continued

REAGENT or RESOURCE	SOURCE	IDENTIFIER
NEBNext Ultra II RNA Library Preparation Kit	New England Biolabs	Cat# E7770
NextSeq500/550 High Output Kit	Illumina	Cat# 20024906
Taqman assay for the mouse *Cyp11a1*	Thermo-Fisher Scientific	Mm00490735_m1
Taqman assay for the mouse *Cyp17a1*	Thermo-Fisher Scientific	Mm00484040_m1
Taqman assay for the mouse *Hsd3b*	Thermo-Fisher Scientific	Mm01261390_m1
Taqman assay for the mouse *Nfatc1*	Thermo-Fisher Scientific	Mm01265944_m1
Taqman assay for the mouse *Acp5*	Thermo-Fisher Scientific	Mm00475698_m1
Taqman assay for the mouse *Itgb3*	Thermo-Fisher Scientific	Mm00443980_m1
Taqman assay for the mouse *Calcr*	Thermo-Fisher Scientific	Mm00432282_m1
Taqman assay for the mouse *Tm7sf4*	Thermo-Fisher Scientific	Mm04209236_m1
Taqman assay for the mouse *C20orf123*	Thermo-Fisher Scientific	Mm00512445_m1
Taqman assay for the mouse *Ctsk*,	Thermo-Fisher Scientific	Mm00484039_m1
Taqman assay for the mouse *P4hb*	Thermo-Fisher Scientific	Mm01243188_m1
Taqman assay for the mouse *Vdac1*	Thermo-Fisher Scientific	Mm00834272_m1
Mouse Competitive ELISA Kit for pregnenolone	Elabscience Biotech.	Cat# E-EL-0086
Mouse Competitive ELISA Kit for aldosterone	Elabscience Biotech.	Cat# E-EL-0070
Mouse Competitive ELISA Kit for corticosterone	Elabscience Biotech.	Cat# E-EL-0161
Mouse Competitive ELISA Kit for estradiol	Elabscience Biotech.	Cat# E-EL-0150
Mouse Competitive ELISA Kit for progesterone	Elabscience Biotech.	Cat# E-EL-0154
Mouse Competitive ELISA Kit DHEA	Elabscience Biotech.	Cat# E-EL-0115
Mouse Competitive ELISA Kit dihydrotestosterone	Elabscience Biotech.	Cat# E-EL-0031
Mouse Competitive ELISA Kit testosterone	Elabscience Biotech.	Cat# E-EL-0155
Mouse Competitive ELISA Kit M-CSF	Elabscience Biotech.	Cat# E-EL-M2445
Mouse Competitive ELISA Kit RANKL	Elabscience Biotech.	Cat# E-EL-M0644
Deposited data		
RNA sequencing data	NCBI BioProject	PRJNA887432
Experimental models: Cell lines		
E0771	ATCC	Cat# CRL-3461
TRAMP-C1	ATCC	Cat# CRL-2730
E0771/Bone	Toru Hiraga	N/A
B16F10	ATCC	Cat# CRL-6475
LLC	Klaus Okkenhaug	N/A
MC38	Klaus Okkenhaug	N/A
A375	ATCC	Cat# CRL-1619
MDA-MB-435S	ATCC	Cat# HTB-129
A549	ATCC	Cat# CRM-CCL-185
NCI-H1299	ATCC	Cat# CRL-5803
NCI-H460	ATCC	Cat# HTB-177
DU145	ATCC	Cat# HTB-81
LNCaP	ATCC	Cat# CRL-1740
PC-3	ATCC	Cat# CRL-1435
Hs895.T	ATCC	Cat# CRL-7637
SK-MEL-28	ATCC	Cat# HTB-72
BEAS-2B	ATCC	Cat# CRL-3588
NCI-H2126	ATCC	Cat# CCL-256
NCI-H128	ATCC	Cat# HTB-120
HCC70	ATCC	Cat# CRL-2315
MCF-10A	ATCC	Cat# CRL-10317

(*Continued on next page*)

Continued

REAGENT or RESOURCE	SOURCE	IDENTIFIER
MDA-PCa-2b	ATCC	Cat# CRL-2422
LASCPC-01	ATCC	Cat# CRL-3356
RWPE-1	ATCC	Cat# CRL-3607
MCF-7	ATCC	Cat# HTB-22
MDA-MB-231	ATCC	Cat# CRM-HTB-26
Experimental models: Organisms/strains		
C57Bl/6 mice	Jackson Laboratory	RRID:IMSR_JAX:000664
Lifeact-eGFP mouse strain	Michael Sixt	N/A
CtskTM 1(cre)Ska mouse strain	Shigeaki Kato	N/A
Gt(ROSA)26SorTM 4(ACTB–tdTomato,–EGFP)Luo mouse strain	Jackson Laboratory	RRID:IMSR_JAX:007676
Tnfrsf11atm1.1Pngr mouse strain	Josef Penninger	N/A
Oligonucleotides		
gRNA1 for pSpCas9-Cyp11a1 CACCTACGGACTTGCTAGGCTCTCT	This paper	N/A
gRNA2 for pSpCas9-Cyp11a1 CAAGGTAAAAGGGTGAACGCTGGCT	This paper	N/A
gRNA3 for pSpCas9-Cyp11a1 CACCAACGAGTTGGGTCAAACTTGT	This paper	N/A
gRNA for lentiCRISPRv2-P4hb 5′-AAGCAACTTCGCGGAGGCGC-3′	This paper	N/A
Recombinant DNA		
pSpCas9 vector (PX459)	Ran et al. *Nat Protoc.* 2013.[43]	Addgene, Cat# 62988
pcDNA3.1 vector	pcDNA3.1 was a gift from Bertrand Collet	Addgene, Cat# 200458
lentiCRISPRv2	Sanjana et al. *Nat Methods.* 2014.[44]	Addgene, Cat# 52961
psPAX2	psPAX2 was a gift from Didier Trono	Addgene, Cat# 12260
pMD2.G	pMD2.G was a gift from Didier Trono	Addgene, Cat# 12259
Software and algorithms		
Leica Application Suite X software	Leica Microsystems	https://www.leica-microsystems.com
SkyScan CT-Analyser software	Bruker	https://www.bruker.com
StrandNGS software	StrandNGS	www.strand-ngs.com
Real-time PCR	Bio-Rad	CFX384
ImageJ/Fiji software	NIH, Bethesda	https://imagej.nih.gov/ij/index.html
FlowJo v10	FlowJo software	https://www.flowjo.com/solutions/flowjo
Microsoft Excel 2016	Microsoft	https://www.microsoft.com

RESOURCE AVAILABILITY

Lead contact

Further information and requests for resources and reagents should be directed to and will be fulfilled by the Lead Contact, Dr. David S. Gyori (gyori.david@semmelweis.hu).

Materials availability

All unique/stable reagents generated in this study are available from the lead contact with a completed Materials Transfer Agreement.

Data and code availability

- All original data reported in this paper are available from the lead contact upon request.
- All raw RNA sequencing data from this study have been submitted to the NCBI BioProject database (https://www.ncbi.nlm.nih.gov/bioproject) under accession number PRJNA887432.
- Any additional information required to reanalyze the data reported in this paper is available from the lead contact upon request.

EXPERIMENTAL MODEL AND STUDY PARTICIPANT DETAILS

Clinical samples

Experiments on human cells were approved by the Semmelweis University Regional and Institutional Committee of Science and Research Ethics and informed consent was obtained from all subjects. Human osteoclasts were differentiated from peripheral blood mononuclear cells of healthy volunteers obtained by dextran sedimentation and Ficoll-Paque gradient centrifugation. Mononuclear cells were washed and plated onto 24-well tissue culture plates or bovine bone slices and cultured in the presence of 20 ng/mL recombinant human M-CSF and 20 ng/mL soluble human RANKL for 2 days, and then in the indicated concentration of pregnenolone or vehicle for 12 days with media changes every 2 days.

Animals

All animal experiments were approved by the Animal Experimentation Review Board of Semmelweis University. C57Bl/6 mice were purchased from Charles River Laboratories. Transgenic mice ubiquitously expressing Lifeact-eGFP[45] were provided by Michael Sixt (Institute of Science and Technology, Klosterneuburg, Austria) and maintained in a homozygous form. Mice carrying the Ctsk$^{TM\ 1(cre)Ska}$ (referred to as Ctsk-Cre) knock-in allele[46] were obtained from Shigeaki Kato (University of Tokyo) and were maintained in heterozygous form. Mice carrying the Gt(ROSA)26Sor$^{TM\ 4(ACTB–tdTomato,–EGFP)Luo}$ (referred to as mTmG) knock-in mutation[47] were obtained from the Jackson Laboratory and were maintained in homozygous form. *Tnfrsf11a*$^{-/-}$ (referred to as RANK-deficient) mice were obtained from Josef Penninger (Institute of Molecular Biotechnology, Austria) and were maintained in heterozygous form.[48] All mice were on the C57Bl/6 genetic background. Mice of both sexes were used and animals were between 8 and 12 weeks of age. Animals were kept in individually ventilated cages in a specific pathogen-free facility.

Cell lines

E0771/Pa breast and TRAMP-C1 prostate carcinoma cells were obtained from ATCC. E0771/Bone cells were obtained from Toru Hiraga (Matsumoto Dental University, Shiojiri, Japan).[12] B16F10 malignant melanoma cell lines were obtained from ATCC. LLC Lewis lung carcinoma cells were obtained from Klaus Okkenhaug (University of Cambridge, Cambridge, United Kingdom), with permission from Matthew Kraman (F-star Biotechnology, Cambridge, United Kingdom). MC38 colon carcinoma cell line was obtained from Klaus Okkenhaug (University of Cambridge, Cambridge, United Kingdom), with permission from Mark Smyth (QIMR Berghofer, Brisbane, Australia). Human cell lines A375, MDA-MB-435S, A549, NCI-H1299, NCI-H460, DU145, LNCaP, PC-3, Hs895.T, SK-MEL-28, BEAS-2B, NCI-H2126, NCI-H128, HCC70, MCF-10A, MDA-PCa-2b, LASCPC-01, RWPE-1, MCF-7 and MDA-MB-231 were obtained from ATCC.

METHOD DETAILS

Deletion and overexpression of the genes encoding CYP11A1 and P4HB

gRNA sequences directed against exon 1 of the murine *Cyp11a1* gene were designed using the CHOPCHOP web tool for genome engineering.[49] Analysis of likely off-target genes was performed *in silico*. No genes directly involved in cell proliferation and differentiation were identified as off-targets. The following CRISPR guide oligonucleotides were ordered: 5′-CACCTACGGACTTGC TAGGCTCTCT-3′ (forward), 5′- AGAGAGCCTAGCAAGTCCGTAGGTG-3′ (reverse), 5′- CAAGGTAAAAGGGTGAACGCTGGCT-3′ (forward), 5′-AGCCAGCGTTCACCCTTTTACCTTG-3′ (reverse), 5′- CACCAACGAGTTGGGTCAAACTTGT-3′ (forward) 5′- ACAAG TTTGACCCAACTCGTTGGTG-3′ (reverse), and subcloned into the pSpCas9 vector (PX459, Addgene). After sequence verification of the inserts, B16F10 tumor cells were transfected with the vectors using Lipofectamine 3000 (ThermoFisher Scientific) transfection reagent. Cells were subsequently selected with 5 μg/mL puromycin for 72 h and used for single-cell clone generation. Genomic modification of single-cell clones was assessed by Western blotting and ELISA. 2 different clones (AB12-183-A1 and CK21-276-H2) were tested *in vitro* and implanted in *in vivo* experiments.

For overexpression of *Cyp11a1* in TRAMP-C1 cells pcDNA3.1 plasmids (Addgene) were used. Cells were transfected using Lipofectamine 3000 (ThermoFisher Scientific) as described by the manufacturer. After transfection, cells stably expressing *Cyp11a1* were selected using 500 μg/mL G418 antibiotic for 4 weeks. Levels of mRNA transcripts and protein expression were monitored by RT-PCR and Western blotting.

P4hb$^{-/-}$ cells were generated using CRISPR/Cas9 mutagenesis. The gRNA sequence targeting P4HB was designed using the CHOPCHOP web tool,[49] as follows: 5′-AAGCAACTTCGCGGAGGCGC-3′. Then, gRNA was cloned into the lentiCRISPRv2 (Addgene, 52961) vector. The constructed lentiCRISPRv2 plasmid together with the packaging plasmids, psPAX2 (Addgene, 12260) and pMD2.G (Addgene, 12259) were transfected into HEK293T cells. The lentiviral particles in the supernatant were harvested and added to wild-type fetal liver cells isolated from C57Bl/6 mice. Mock transduced cells (with empty vectors) were used as controls and the transfected cells were selected with blasticidin. Then, genomic DNA of the cells was isolated for sequencing, and protein was extracted for immunoblotting with anti-P4HB antibody (Abcam, ab2792).

Tumor models

Tumor cells were maintained in culture in DMEM containing 10% FCS (Gibco). Tumor cell supernatants were centrifuged at 3000 g for 20 min, filtered through 0.22 pore diameter filters (Corning), and supplemented with empty αMEM medium before using it in cell culture experiments. Suspensions of tumor cells were prepared in sterile PBS, and cell counts were determined manually using Neubauer chambers. For primary tumor growth measurements, 0.5 x 10^6 E0771/Bone or 1 x 10^5 B16F10 cells were administered in 100 μL PBS into the mammary fat pads or by intradermal injections in the skin of the shaved left flank of isoflurane-anesthetized C57Bl/6 mice, respectively. When tumors became palpable (around day 7–10), tumor growth was monitored by caliper measurements every 2–3 days. Tumor volume (mm^3) was calculated as length x $width^2$. Mice bearing tumors were culled at 21 days after implantation. Any mice bearing tumors that approached or exceeded the terminal size limit (10% of the weight of the mouse at the start of the study) during the course of the study were culled and excluded from the study.[50,51] Tumor-bearing mice were treated with 50 mg/kg 2-AG orally every 2 days. For lung and bone metastasis formation, 0.5 x 10^6 E0771/Bone or 1 x 10^5 B16F10 cells were administered in 100 μL PBS into the tail vein or caudal artery[52] of C57Bl/6 mice, respectively.

Micro-CT and histomorphometric analyses

Trabecular bone structure and mineralization were tested by micro-CT analysis of the distal metaphysis of the femurs of tumor cell-injected C57Bl/6 mice as previously described.[53–55] Micro-CT sections were acquired using a SkyScan 1172 micro-CT apparatus (Bruker, Kontic, Belgium) with an isometric voxel size of 4.5 μm, followed by reconstitution of a three-dimensional axial cylinder of 700 μm diameter expanding from 150 to 450 sections proximal to the distal growth plate, and calculation of quantitative micro-CT parameters using the SkyScan NRecon and CT-Analyser softwares.[53–55]

Histomorphometry studies were performed on the distal metaphysis of the femurs of tumor cell-injected C57Bl/6 mice as previously described.[54] Bones were fixed in PBS with 4% PFA, decalcified in OSTEOSOFT (Merck/Sigma), embedded in paraffin, sectioned and stained with tartrate resistant acid phosphatase (TRAP) and hematoxylin-eosin stains (Merck/Sigma). Histomorphometric analysis was performed using a Leica DMI6000B inverted microscope according to international standards.[56]

In vitro and *in vivo* mouse macrophage and osteoclast cultures and resorption assays

Wild type macrophages were generated by isolating bone marrow cells from the long bones (femurs, tibias) of C57Bl/6 mice and then cultured in the presence of 20 ng/mL M-CSF.

Osteoclast cultures were performed essentially as previously described.[53–55] Wild type, Lifeact-eGFP, Ctsk-Cre or mTmG osteoclast precursor cells were cultured in the presence of 20 or 50 ng/mL mouse recombinant M-CSF and 20 or 50 ng/mL soluble RANKL for 2 days and then in the presence of the indicated concentration of pregnenolone or vehicle for 3 more days. Osteoclast morphology was tested by a commercially available TRAP staining kit (Merck/Sigma) on day 5. Images were made by using a Leica DMI6000B inverted microscope and the number of osteoclasts (defined as TRAP-positive cells with 3 or more nuclei) was counted manually. For *in vitro* resorption assays, osteoclasts were cultured under similar conditions for 11 more days with media changes every 2–3 days on artificial hydroxyapatite layer (BD BioCoat Osteologic slides) or on bovine cortical bone slices (Immunodiagnostic Systems), followed by toluidine blue staining and determination of the resorbed area using ImageJ software (NIH).

For osteoclast-tumor cell co-culture experiments, wild type bone marrow-derived osteoclast precursors were cultured in the presence of 20 ng/mL recombinant mouse M-CSF and soluble RANKL for 2 days. Then B16F10 tumor cells were added to the cultures at a density of 5×10^4 cells/cm^2. Osteoclast morphology (TRAP expression) and resorptive function were then determined as described above. Tumor cell supernatants were also added to the cultures after 2 days of initial recombinant M-CSF and soluble RANKL treatments.

3×10^6 WT and *P4hb*$^{-/-}$ fetal liver cells were intravenously injected into *Tnfrsf11a*$^{-/-}$ (RANK-deficient) neonates at postnatal days 5, 7 and 9. 8 weeks later, micro-CT and histomorphometric analysis of the distal femoral metaphysis of the animals was carried out as previously described.[53–55]

Detection of cell survival and OC-STAMP surface expression

For flow cytometry analysis, pre-osteoclasts were obtained by culturing mouse bone marrow-derived macrophage precursors for 2 days in the presence of 20 ng/mL M-CSF and 20 ng/mL soluble RANKL or the indicated concentration of pregnenolone with or without quercetin-3-rutinoside. Cells were suspended by 0.25% Trypsin-EDTA (Merck/Sigma), stained with Annexin-V-PE and 7-amino-actinomycin D (both from BD Pharmingen) or FITC-labeled anti-OC-STAMP-mAb (NBP1-78156, Novus Biologicals) according to the manufacturer's instructions and analyzed on a BD FACSCalibur flow cytometer.[54]

Actin ring formation assay

For the detection of acting rings, bone marrow-derived macrophage precursors obtained from wild-type or Lifeact-eGFP transgenic mice were cultured in the presence of 20 ng/mL M-CSF and 20 ng/mL soluble RANKL for 2 days and then with or without the indicated concentration of pregnenolone for another 3 days. Images were taken using a Leica DMI6000B fluorescence microscope as previously described.[54] For detection of nuclei, cells were fixed with 4% paraformaldehyde and stained with 1:1000 DAPI (Invitrogen).

In vitro osteoclast fusion assay

For the detection of osteoclast fusion, Ctsk-Cre and mTmG bone marrow cells were co-cultured in the presence of 20 or 50 ng/mL mouse M-CSF and 20 or 50 ng/mL mouse soluble RANKL for 2 days and then with 200 nM pregnenolone or vehicle for another 3 days. For real-time time-lapse video microscopy, cell cultures were incubated with 5% CO_2–95% air gas mixture, humidity and a constant temperature of 37°C as previously described.[22] Images were taken using a Leica DMI6000B fluorescence microscope every 60 min. Real-time images and videos were processed using ImageJ/Fiji.

RNA sequencing and quantitative PCR

Total RNA from E0771/Pa and E0771/Bone cells were converted into RNA-Seq libraries with the NEBNext Ultra II RNA Library Preparation Kit (New England Biolabs, Ipswich, MA, USA). Sequencing was performed on Illumina NextSeq500 instrument using the NextSeq500/550 High Output Kit v2.5 (75 cycles) as previously described.[57] Hisat2 algorithm was used for alignment and raw sequencing reads were mapped to the Mm10 mouse reference genome and BAM files were generated. Downstream analysis was performed using StrandNGS software (www.strand-ngs.com). BAM files were imported into the software DESeq algorithm was used for normalization. Moderated T test was used for determine differentially expressed genes, p values were corrected by the method of Benjamini and Hochberg false discovery rate to take multiple testing into account. Gene ontology and pathway enrichment analysis was performed essentially as described before.[57]

To detect gene expression changes with qPCR, tumor cells were cultured in DMEM with 10% FBS or mouse bone marrow progenitors were cultured for 2 days in the presence of 20 ng/mL M-CSF with or without soluble RANKL and then for 3 days in the presence of the indicated concentration of pregnenolone or vehicle, followed by RNA extraction and reverse transcription as previously described.[53,54] Quantitative PCR was then performed using Taqman assays for the mouse *Cyp11a1, Cyp17a1, Hsd3b, Nfatc1, Acp5*, *Itgb3*, *Calcr*, *Tm7sf4*, *Ocstamp, Ctsk, P4hb, Vdac1* genes and transcript levels relative to *Gapdh* were calculated using the comparative C_t method.

In vitro wound healing and migration assays

For wound healing assays, wild-type bone marrow-derived osteoclast precursors were grown in the presence of 20 ng/mL mouse M-CSF and RANKL to reach 90–95% confluence. Then, the monolayer of cells was scraped with a standard 200 μL sterile micropipette tip to create a denuded gap of constant width. The cells were subsequently exposed to 20 ng/mL mouse M-CSF and RANKL with or without pregnenolone for 24 h and imaged every 8 h under constant conditions (5% CO2–95% air gas mixture, humidity and temperature of 37°C) using a Leica DMI6000B microscope.

For *in vitro* migration experiments, Transwell inserts with a polycarbonate membrane with 5 μm pore size (Corning) were precoated with fibrinogen as previously described[58] and filled with pre-osteoclast cell suspensions. The inserts were placed into 24-well plates filled with the indicated concentrations of mouse recombinant M-CSF and soluble RANKL with or without pregnenolone. After 60 min, the plates were spun, the inserts were removed, and the number of pre-osteoclasts in the bottom of the wells was determined.[58]

Steroid measurement by liquid chromatography mass spectrometry (LC-MS/MS)

Liquid chromatography and mass spectrometry steroid measurements were carried out essentially as described before.[59] Samples (100 μL) of each cell supernantant sample was enriched with isotopically labeled internal standards, including $^{13}C_2$,d2-pregnenolone (1 ng) and extracted along with a mixed steroid calibration curve, including pregnenolone (0.005–1 ng) through supported liquid extraction plates on an Extrahera liquid handling robot (Biotage, Uppsala, Sweden) using dichloromethane/isopropanol (98:2 v/v), reduced to dryness under nitrogen and resuspension in water/methanol (80 μL; 70:30 v/v water/methanol) followed by LC-MS/MS analysis of the extract. Briefly, an I-Class UPLC (Waters, UK) was used for the liquid chromatography on a Kinetex C18 column (150 × 2.1 mm; 2.6 μm) with a flow rate of 0.3 mL/min and a mobile phase system of water with 0.05 mM ammonium fluoride and methanol with 0.05 mM ammonium fluoride, starting at 50% B, rising to 95% B and returning to 50% B. Separation of 18 steroids was carried out (Figure S1E) The column and autosampler temperatures were maintained at 50 and 10°C, respectively. The injection volume was 20 μL and the total analytical run time per sample was 16 min. Steroids were detected on a QTrap 6500+ mass spectrometer (AB Sciex, Warrington, UK) equipped with an electrospray ionisation turbo V ion spray source. Positive ion spray voltage was set to 5500 V and negative ion spray voltage was set to −4500 V, with the source temperature maintained at 600°C. Multiple reaction monitoring parameters were carried out for all steroids including pregnenolone (P5) *m/z* 317.1 281.1 and 159.0 with declustering potential (DP) of 66 collision exit potential (CXP) of 31 and 29 V and collision energy (CE) of 12 V, respectively and for $^{13}C_2$,d2-pregnenolone of 321.2 → 285.2 with DP of 14 CXP of 17 and CE of 18 with retention time of 10.4 min.

The ratio of P5/$^{13}C_2$,d2-P5 peak areas were calculated and linear regression analysis used to calculate the amount of P5 in each sample. The same was done for other steroids in the sample (aldosterone, cortisol, DHEA, androstenedione, progesterone, 17β-estradiol, estron, estriol, 5α-dihydrotestosterone and testosterone) by evaluation of the data on MultiQuant 3.0.3 (AB Sciex, UK).[59]

Immunoblotting and ELISA

Immunoblotting was performed as previously described.[60] Cells were washed with ice-cold PBS and lysed using radioimmunoprecipitation assay buffer (RIPA, containing 1% Triton X-, 0.1% SDS, 0.5% sodium deoxycholate, 30 mM HEPES, 5 mM Na-EGTA, 10 mM benzamidine, and 20 mM NaF in physiological saline) supplemented with sodium-orthovanadate, phosphatase inhibitor cocktails 1 and 2, PMSF and aprotinin (all from Merck/Sigma-Aldrich). Cell debris was removed by centrifugation at 16,000 g. 4x reducing sample buffer was added for the samples and boiled for 10 min 20 μg of total protein was run on a 14% SDS-polyacrylamide gel, electroblotted onto nitrocellulose membranes and stained with Ponceau. Membranes were then blocked with 3% dry milk in PBS and 0.1% Tween 20 (PBS-Tween), followed by immunoblotting with primary antibodies against Cyp11a1 (1:1000, ab175408, Abcam) or β-actin (1:10000, Clone AC-74; Merck/Sigma) diluted in 3% BSA in PBS-Tween, followed by HRP-labeled anti-rabbit IgG and anti-mouse IgG antibodies (1:5000, GE Healthcare) diluted in 3% dry milk in PBS-Tween. Signal was developed by ECL (GE Healthcare) and exposed to X-ray film.[60]

Levels of pregnenolone, aldosterone, corticosterone, estradiol, progesterone, 17-OH pregnenolone, DHEA, androstenedione, dihydrotestosterone, testosterone, M-CSF and RANKL present within the supernatants of tumor cells were measured using the Mouse Competitive ELISA Kits (Elabscience Biotechnology Ltd.), in accordance with the manufacturer's instructions and as previously described.[50]

QUANTIFICATION AND STATISTICAL ANALYSIS

All experiments were performed 3 or more times (or on at least 6 individual mice per group) with comparable results. Statistical analysis was performed using Student's unpaired two-population t test or 2-way, repeated-measures ANOVA with Bonferroni's post hoc test. Differences with p values of <0.05 were considered statistically significant: *, $p < 0.05$; **, $p < 0.01$; ***, $p < 0.002$; ****, $p < 0.0004$.